# The Volyn biota (Ukraine) – indications for 1.5 Ga old eukaryotes in 3D-preservation, a spotlight on the 'boring billion'

Gerhard Franz[1], Vladimir Khomenko[2], Peter Lyckberg[3], Vsevolod Chournousenko[4], Ulrich Struck[5], Ulrich Gernert[6], Jörg Nissen[6]

[1]Institut für Angewandte Geowissenschaften, Technische Universität Berlin, D-10587 Berlin, Germany

[2]M.P. Semenenko Institute of Geochemistry, Mineralogy and Ore Formation, The National Academy of Sciences of Ukraine, 34, Palladina av., Kyiv, 03142, Ukraine

[3]Luxembourg National Museum of Natural History, 25 Rue Münster, 2160 Luxembourg, Luxembourg

[4]Volyn Quartz Samotsvety Company, Khoroshiv (Volodarsk-Volynski), Ukraine

[5]Museum für Naturkunde, Leibniz-Institut für Evolutions- und Biodiversitätsforschung, Invalidenstraße 43, Berlin, D-10115, Germany

[6]Zentraleinrichtung Elektronenmikroskopie, Technische Universität Berlin, D-10623 Berlin, Germany

Correspondence to: Gerhard Franz (gefra548@gmail.com; gerhard.franz@tu-berlin.de)

**Abstract**

The Volyn biota, fossilized organisms with a minimum age of 1.5 Ga, were found in cavities in granitic pegmatites from the Korosten pluton, NW Ukrainian shield. Fossilization was due to influx of hydrothermal fluorine-rich waters, which silicified the outermost part of the organisms, thus preserving the 3D morphology. Details of the morphology (investigated by scanning electron microscopy) show that the majority of the specimens is filamentous, of a large variety with diameters ranging from ~10 µm to ~200 µm, thin filaments with typical branching, thick filaments with ball-shaped outgrowths and dented surface. Filaments can be straight or conical, curvilinear or strongly curved, up to mm in length, some with a central channel. Some filaments show indications for segmentation, are grown as sessile organisms onto substrate; others show both intact ends, indicating a non-sessile, free-living lifestyle. Objects with flaky morphology and agglutinating filaments are interpreted as fossil biofilms. Other objects are hollow and show a large variety of forms; spherical objects are scarce. Infrared spectroscopy indicates the presence of chitosan in one filament type, electron microprobe analysis of nm-sized inclusions in filaments identified the presence of Bi(Te,S) minerals, and

**Gelöscht:** growth in soft medium or planktonic organisms

both observations are compatible with the interpretation as fungi-like organisms. Stable C- and N-isotope data of bulk samples are in the range of -31 to -47 ‰ $\delta^{13}C$, and of +3 to +10 ‰ $\delta^{15}N$, indicating possible methanogens as part of the subsurface micro-ecosystem. The Volyn biota indicate that at 1.5 Ga complex forms of life existed in the continental deep biosphere, well above the microscopic level, including fungi-like organisms resembling eukaryotes.

Gelöscht: show

Gelöscht: eukaryotes

Gelöscht: lived in the continental deep biosphere, where complex forms of life existed, well above the microscopic level

## 1 Introduction

Precambrian fossils are generally not well preserved because of the absence of skeletal parts. In addition, most Precambrian fossil record is from sedimentary rocks with strong diagenetic or even metamorphic overprint, which destroyed much of the original morphology and in extreme cases of very old organisms left only an isotopic signature (e.g. Alleon et al., 2018; Berbee et al., 2020). Therefore, their biogenicity is often disputed especially when the organic matter (OM) is completely replaced, often by silica or pyrite. A preservation of 3D-morphology is very rare and requires special fossilization conditions, which include first prevention of rapid decay of the OM and then preservation of the space around the fossil in order to preserve its original morphology. These conditions were fulfilled in pegmatites of the Volyn pegmatite field, Ukraine, associated with the Korosten Pluton. These so-called 'chamber pegmatites' contain large miarolitic cavities in which OM named (oxy)-kerite was found and in previous investigations interpreted as an example of a-biogenic formation (Ginzburg et al., 1987; Luk'yanova et al., 1992), later re-interpreted as fossil cyanobacteria (Gorlenko et al., 2000; Zhmur, 2003) from a geyser type deposit. Ginzburg et al. (1987) give a composition of 60-76 wt% C, 5-7 wt% H, 9-23 wt% O, 8-9 wt% N, and 2-3 wt% S and an empirical formula of $C_{491}H_{386}O_{87}(S)N$. Gorlenko et al. (2000) and Zhmur (2003) mention masses of up to 3 kg of kerite in one of the cavities with an irregular distribution within the pegmatite.

The organisms lived in these cavities and provide an example of the Precambrian deep biosphere. Their fossilization conditions included sudden influx of hot hydrothermal waters in the geyser system, where magmatic fluids rich in $SiF_4$ mixed with meteoric waters (Franz et al., 2022a), infiltration of Si-Al into the outermost layer of the fossils, and formation of dominantly clay mineral encrustations. The 1.76 Ga intrusion age of the pegmatites (U-Pb zircon; Shumlyanksyy et al., 2021) provides a maximum age of the fossils; the minimum age of 1.5 Ga is provided by the age of formation of a breccia, which contains degraded OM, brown opal with OM, buddingtonite which $NH_4$-content was provided by the degraded OM, and muscovite ($^{40}Ar$-$^{39}Ar$ laser ablation data; Franz et al., 2022b). An additional argument for this age comes

from the brown opal, which cements the breccia and contains organic matter (Franz et al., 2017, and references therein). Therefore, we assume that breccia formation must have occurred when organic matter was already present in the 'chambers'. Although some of the miarolitic chambers collapsed, producing the muscovite-opal-bearing breccia, other chambers are still intact and were mined since the 1930ies for piezo quartz and until now for pegmatite minerals such as beryl and topaz (Ivanovich and Alekseevich, 2007; Lyckberg et al., 2009, 2019).

We report here details about the morphology and the internal structure of the fossils, investigated by scanning electron microscopy (SEM) and electron microprobe analysis (EMPA), and provide stable C-N isotope and infrared spectroscopy (FTIR) data, which allow speculating about the types of organisms. An important point is that these 'micro'-fossils in many cases reach a size well above the microscopic level, with filaments of several mm in length. The age of the fossils of 1.5 Ga in the middle of the 'boring billion' and gives insight into the organisms of the deep continental biosphere.

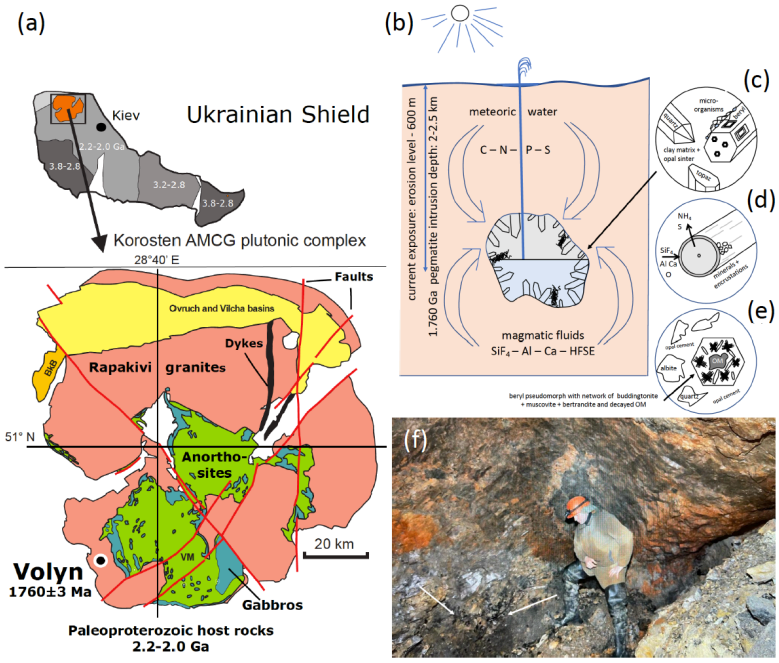


**Fig. 1 (a) Location of the Volyn pegmatite field in the Ukrainian shield, which hosts the Volyn biota. (b) Conceptual model for the fossilization in the miarolitic cavities ('chambers') in the pegmatite. Current exposure is from the erosion level to a depth of 600 m. Kerite is attached to the walls, often to feldspar, but also (c) on topaz and beryl crystals. (d) Fossilization produces a thin rim of Si-Al enrichment and encrustations of clay minerals. (e) In collapsed chambers, a breccia formed with pseudomorph of**

**buddingtonite+muscovite+opal after beryl. Decaying kerite produced $NH_4$ for formation of buddingtonite. The Ar-Ar-LA age of muscovite is considered as minimum age for the fossils. (f) View into a chamber, arrows point to black kerite; (all images reproduced from Franz et al., 2022a).**

## 2 Geological framework and sample material

The locality in the Ukrainian Precambrian shield is associated with the Korosten anorthosite-mangerite-charnockite-granite plutonic complex (Shumlyanksyy et al., 2012) (Fig. 1). The samples were recovered from underground in shaft 3 of the mine from a depth of approximately 100 m, one sample was obtained from the mineralogical museum of the Academy of Sciences, Kiev, and one beryl sample with kerite on beryl was collected from the mine tailings (Table 1). Two additional samples of topaz from the museum in Kiev with kerite (Fig. 2) were not investigated in detail. The samples from underground could be simply picked up with no need for separation from rock matrix and were stored in plastic sample bags. Kerite has not been found outside the cavities, which are in the core of the pegmatite. It exists as fine fiber masses between fragments of the wall of the cavities and as larger masses hanging freely on the walls, attached to feldspar and often around topaz (Fig. 2b, c) and to beryl (Fig. 2d-j). The bottom of the cavities is covered with soft clay.

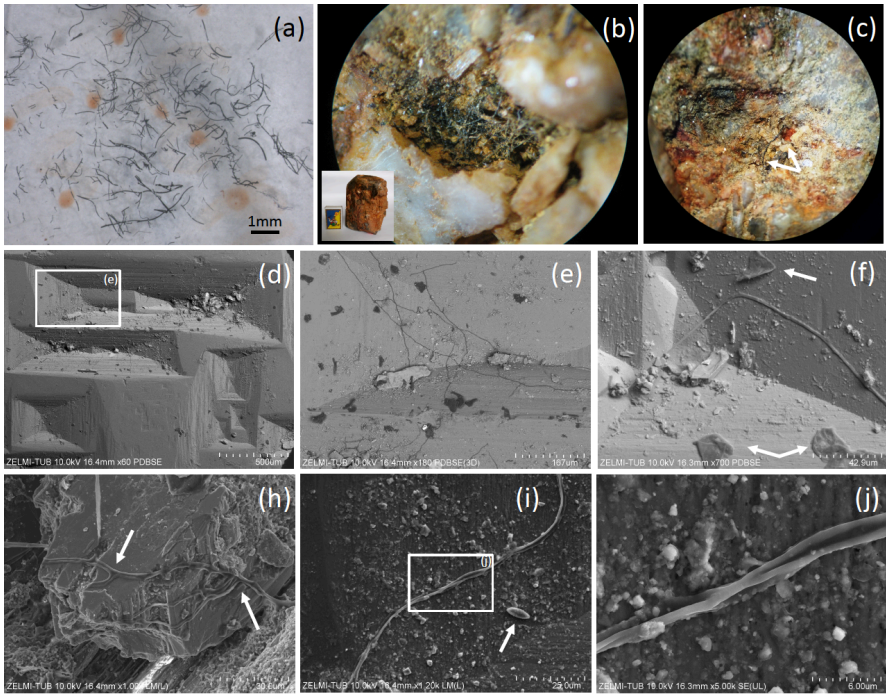

**Fig. 2 (a) Photograph of sample #0, illustrating the pieces of broken, solitary kerite filaments of mm-length. (b) Photograph of kerite filaments on topaz (white crystals with Fe-oxide-hydroxide staining; inset shows topaz crystal with 5-cm large matchbox for scale, image diameter approximately 2 mm). (c) Filaments of different diameter on topaz (arrows; image diameter approximately 3 mm). (d) SEM image (with combined back scattered mode) of beryl prism surface with characteristic etch pits. Rectangle indicates position of (e), which shows filamentous kerite together with kerite in irregular shape (dark contrast indicates organic matter). (f) SEM image, arrows point to kerite with irregular shape. (h) Kerite filaments with branching (arrows) in dissolution feature of beryl. (i) Kerite filament and spherical kerite (arrow) in an etch pit of beryl; rectangle indicates position of (j), illustrating the irregular diameter of the filament.**

The sample #0 consists of broken filaments of several mm length (Fig. 2a) and it is likely that the original length was much larger on the cm scale. It was also found grown onto a topaz crystal (Fig. 2b, c). On beryl it was found attached to dissolution features on the surface of the crystals, but not only in the common filamentous form, but also in irregular shape (Fig. 2d-j) and rarely in spherical shape (Fig. 2i). Although the previous reports mention mostly filaments with smooth surface, our new observations revealed a large variety of different types of filaments, described below.

## 3 Methods

The samples were investigated by SEM and EMPA. SEM images were obtained with a Hitachi SU8030 instrument, equipped with an EDAX EDS system with a 30 $mm^2$ silicon drift detector (SDD) fitted with a silicon nitride window. Samples were coated with an approximately 5 nm thick Ir layer allowing for high-resolution imaging of the filaments' surfaces without the structure of commonly applied Au coating. The kerite samples without further cleaning or preparation were mounted on Al stubs stickered with conductive carbon tabs. The beryl crystals with kerite filaments were dust-cleaned with compressed air and coated with C.

Table 1: List of samples

| No./GFZ no. | Year of sampling | Material | Location |
|---|---|---|---|
| 0/Museum Ac. Sci. Kyiv | unknown | kerite | unknown |
| 1/G017809 | 2018 | kerite | shaft 3 |
| 2/G017810 | 2018 | kerite | shaft 3 |
| 3/G017811 | 2018 | kerite | shaft 3 |
| 4/G017812 | 2018 | kerite | shaft 3 |
| 5/G017813 | 2013 | kerite | shaft 3 |
| 6/G017814 | 2013 | kerite | shaft 3 |
| 7/G017815 | 2013 | kerite | shaft 3 |

| | | | |
|---|---|---|---|
| 2008-V-10 | 2008 | beryl crystal with etch pits | mine tailings pegmatite #2 |

The JEOL JXA-8530F field emission electron microprobe at TU Berlin was used to investigate mounts embedded in epoxy, but with C-coating, for quantitative results and less absorbance (compared to Ir). EPMA data for element distribution maps of cross sections or of parts of the rim of the filaments and flaky kerite were acquired in the wave-length dispersive mode using an 8 kV, 20 nA beam with a probe diameter of 64 nm. Back-scattered electron images (BSE) were taken to select appropriate sites. Mappings were done in stage scan-modus with pixel resolution between 277 and 360 x 180 and 265, with a pixel size of mostly 80 nm, and a dwell time per pixel of 200 ms. Total scan areas varied between 70 x 36 µm to 33.2 x 31.8 µm.

Stable isotope analysis and concentration measurements of nitrogen and carbon were performed simultaneously with a THERMO/Finnigan MAT V isotope ratio mass spectrometer, coupled to a THERMO Flash EA 1112 elemental analyzer via a THERMO/Finnigan Conflo IV- interface in the stable isotope laboratory of the Museum für Naturkunde, Berlin. Isotope ratios are expressed in the conventional delta notation ($\delta^{13}C$ / $\delta^{15}N$) relative to atmospheric N (Mariotti, 1983) and VPDB (Vienna PeeDee Belemnite standard). Standard deviation for repeated measurements of lab standard material (peptone) is generally better than 0.15 per mill (‰) for both N and C. Standard deviations of concentration measurements of replicates of our lab standard are <3% of the concentration analyzed.

FTIR absorption spectra of several small, 40-60 µm wide, translucent dark-brown fragments of kerite (sample #0, which showed the least mineralization crust) were measured in the spectral range 7000 – 700 $cm^{-1}$ at room temperature using a Bruker IFS 66 spectrometer equipped with an IR-microscope. The kerite fragments were selected under a binocular microscope and placed on an IR-transparent KBr plate. Spectra were taken in the transmittance mode at a spectral resolution of 4 $cm^{-1}$ with a measuring spot diameter of 40 µm. The reference spectra were measured through the same KBr plate. The time-averaged signal was collected over 200 scans in both reference and sample spectra. For comparison, absorption spectra of chitin (poly-(1,4)-β-N-acetyl-D-glucosamine) and >75% deacetylated chitin, or chitosan (2-amino-2-deoxy-(1,4)-β-D-glucopyranan, both produced by Sigma-Aldrich Chemie GmbH (C7170-100G, C3646-10G) from shrimp shells, were measured in several single flattened, 30-50 microns thick transparent flakes of these materials at the same conditions. Band assignments are based on literature comparison (Table 1 Supplement).

## 4 Results

### 4.1 Morphology

#### 4.1.1 Filaments

Filaments are curvilinear with smooth surfaces and circular cross section (Fig. 3) with different types of ends (Fig. 4). Other types have a structured surface, some are conical, others strongly curved (Figs. 5, 6). Branching is typical for filaments with smooth surface, and was observed as Y-, T-, and double-T-branching (Fig. 3b, h), as multiple branching (Fig. 3c), and combined Y-T-branching (Fig. 3d). Clear indications for anastomosing filaments were not found. Multiple branching represents the beginning of growth of filaments (Fig. 3e). In others, globular outgrowths possibly mark the beginning of new branches (Fig. 3g). Whereas the diameter of the individual filaments can be homogeneous between approximately 10 µm and 20 µm (sample #0), others (e.g. sample #3; Fig. 3f) show different diameters, between a few µm and several tens of µm. Ball-shaped outgrowths at the end of a filament occur together with a conical thinning-out filament (sample #1; Fig. 3i). Conical, thinning out filaments originate in Y-branching from a thicker filament with constant diameter (Fig. 3m). One object was identified with multiple conical filaments, with claw-like curved ends (sample #6; Fig. 3j, k, l). The bottom part can be interpreted as beginning of growth of the filaments on a substrate, i.e. the clay mineral assemblage in the miarolitic cavities.

Most filaments are broken pieces of larger filaments, and preserved length is in the order of mm, and it can be assumed that the original length was up to cm. Complete filaments were observed, with one end ball-shaped, the other end thinning out (Fig. 6i, o). Whereas beginning of a filament is rarely observed, ends are frequently preserved (Fig. 4) and can be either simply round (Fig. 4a), ball-shaped (Fig. 4b-f), rarely with oval shape (Fig. 4e), or conical-thinning out (Fig. 4g, l, m).

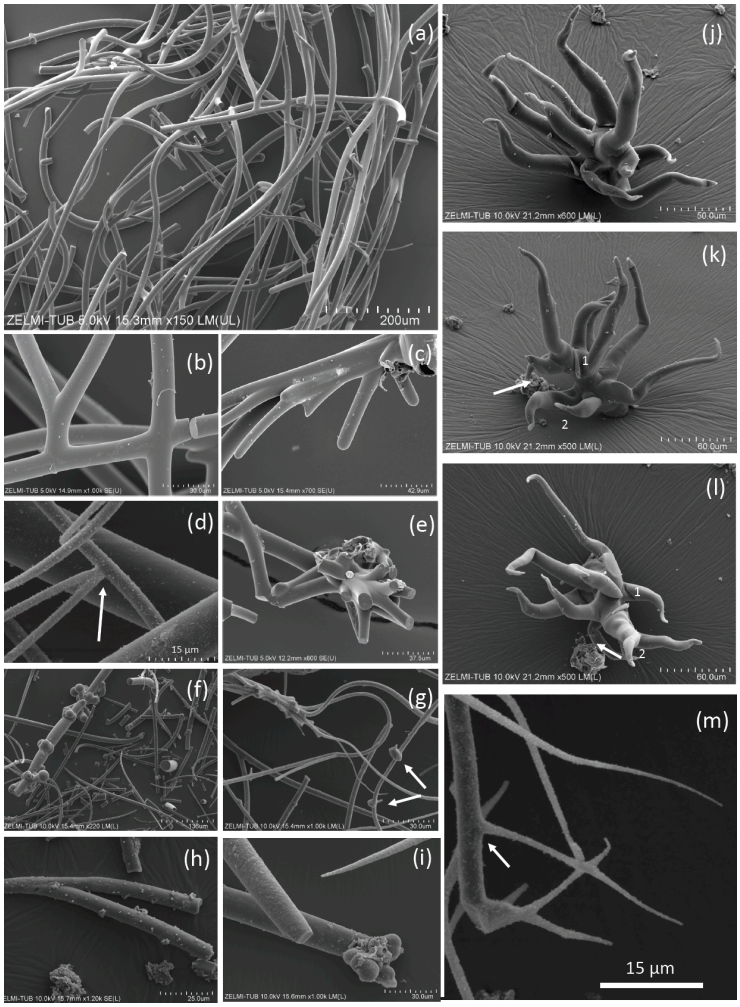


**Fig. 3 SEM images of curvilinear filaments with smooth surfaces and circular cross section. (a) Overview of sample #0, illustrating the amount of material with homogeneous diameter of approximately 10 µm, length of more than 1 cm, round ends. (b) Branching with Y-, T- and double-T-junctions. (c) Multiple branching and (d) combined Y- and T-branching. (e) Possible multiple branching representing the beginning of the filaments. (f) Overview (sample #3) with filaments of variable diameter and (g) multiple branching (upper left) and small outgrowths (arrows). (h) Sample #4 with Y-branching. (i) Sample #1 showing 3 filaments, one thinning out (upper left), one with constant diameter with ball-shaped outgrowths on end (below), and a slightly conical one (above). (j, k, l) Image of multiple, conical filaments with claw-like ends, growing from a common center; view of the same object (sample #6) in different perspectives. In (k) and (l) numbers 1 and 2 identify the same beginning and end of a filament; arrows point to a fluorite crystal. (m) Y-branching of a thinning-out filament (arrow) starting from a filament with constant**

**thickness. The star-like shape in the center is not branching, it shows different filaments in different heights.**

Ball-shaped outgrowths (Fig. 4h) and multiple ball-shaped ends (Fig. 4i) possibly mark the beginning of new branches, and balls can be situated asymmetrically at the end of a filament (Fig. 4j). The structured surface of this ball-shaped end is caused by the fossilization process, as indicated by the round pores in the surface, together with mineral incrustations (Fig. 4k). This is also seen on the surface of a 300 µm long conical filament fragment (Fig. 4m, n), which has a µm-wide rim of mineral incrustations with a homogeneous interior part (Fig. 4o).

The structured surface is only partly a result of the fossilization process. Figure 5a-f shows a filament with approximately 4 mm preserved length and oval cross section (120x80 µm thick on one end), which has a dented surface and bulbous outgrowths (Fig. 4d). Another example of a strongly curved filament (Fig. 4g-l) with bulbous surface, several mm in length and near to 200 µm diameter shows irregular segmentation in distances between 35 µm and 70 µm. On the surface of the filament, relicts of a sheath are visible, partly the sheath is intact. The transition between the intact sheath and the remnants exhibits a polygonal structure and circular 1-2 µm wide holes, probably caused by decay/fossilization. Segmentation is also seen in a branched filament with approximately 3-5 µm wide ridges (Fig. 4m, n, o). This filament has a mineralized outer part of clay minerals with irregular ridges; however, where branching starts, the surface is intact. We interpret these irregular ridges as irregular segmentation of the filament, accentuated and emphasized by fossilization.

Some samples have joint occurrence of filaments with smooth, slightly, and strongly bulbous surfaces (Fig. 6a, b), and joint occurrence of straight, slightly, and strongly curved filaments with irregular segmentation (Fig. 6c, d). The strongly bulbous filaments are transitional to outgrowths (Fig. 6d). Segmentation is indicated (Fig. 6e) and the surface can be strongly sculptured. The filaments have variable diameters from 75 µm (Fig. 6e) to approximately 250 µm (Fig. 6d, f). Some thin filaments show clear indication for segmentation (Fig. 6g, h). The strongly sculptured surface consists of small ball-shaped outgrowths. Joint occurrence of filaments with strongly sculptured surface and smooth surface and with slight striation perpendicular to filament length, and filaments with strong sculptured surface (Fig. 6k, l, m, n), indicates that these are probably different types of organisms, not different stages of fossilization.

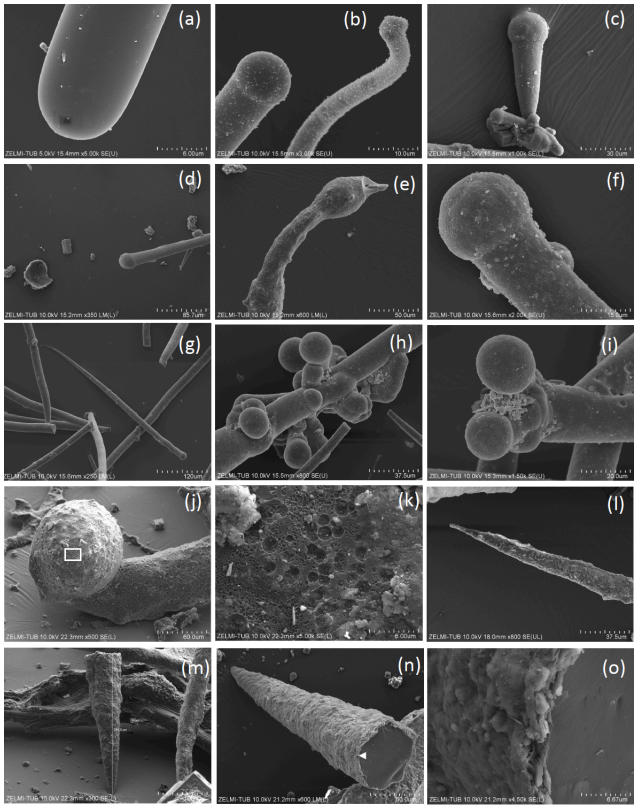


**Fig. 4 SEM images of ends of filaments with smooth surface. (a) Simple round end (sample #0). (b) Ball-shaped end of straight and curved filament (sample #3). (c) Ball-shaped end of conical filament (sample #1). (d) Ball-shaped end of straight filament (sample #5). (e) Oval-shaped outgrowths near end of filament (sample #7). (f) Ball-shaped end (sample #1). (g) Complete filament with one end thinning out, one with a round end (sample #1). (h) Ball-shaped outgrowths and ends (sample #3). (i) Double ball at end of filament (sample #1) (j) Ball-shaped end; rectangle indicates position of (k), surface of the ball with mineral incrustations and porosity, interpreted as result of decay/fossilization (sample #6). (l) Thinning-out of a filament (sample #5). (m, n) Cone-shaped filament in different perspective, approximately 300 µm preserved length (sample #6); white rectangle indicates position of (o) detail of the 1-2 µm wide rim with mineral incrustations.**

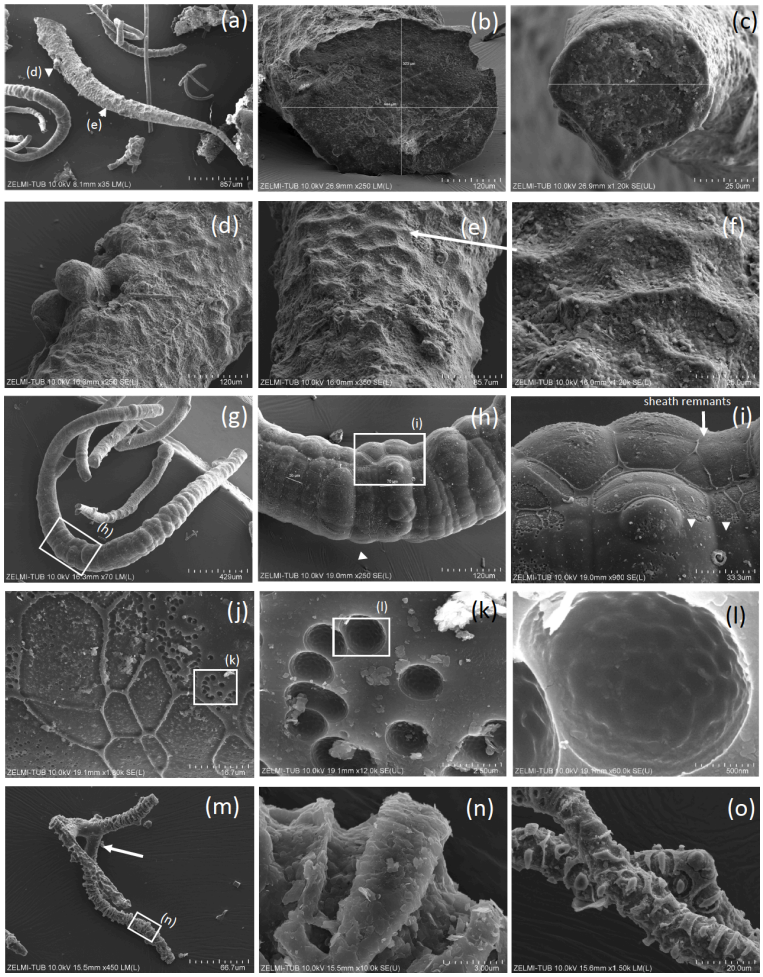


**Fig. 5 Filaments with structured, rough surface. (a) Conical filament of approximately 4 mm preserved length, upper oval diameter (b) 440 µm x 320 µm, (c) thin end 70 µm (sample #5); triangles point to details shown in (d), bulbous outgrowths, and (e, f) dented surface. (g) Strongly curved filament with bulbous surface, several mm in length and near to 200 µm diameter (sample #5). Rectangle shows position of (h), bulbous surface with irregular segmentation in distances between 35 µm and 70 µm; rectangle indicates position of (i), white triangle to position of (j). (i) In the upper part of the filament, relicts of a sheath are visible (single arrow), in the lower part the sheath is intact (triangles point to the contact). (j) The transition between the intact sheath and the remnants in the lower part of the filament exhibits a polygonal structure and (k, l) circular 1-2 µm wide holes, probably caused by decay/fossilization. (m) Branched filament with approximately 3-5 µm wide ridges (sample #2). Note intact surface where branching starts (arrow). (n) Detail of central part of (m). Platy objects are clay minerals. (o) Similar feature of filament surface (sample #4) with irregular ridges, indicating irregular segmentation.**

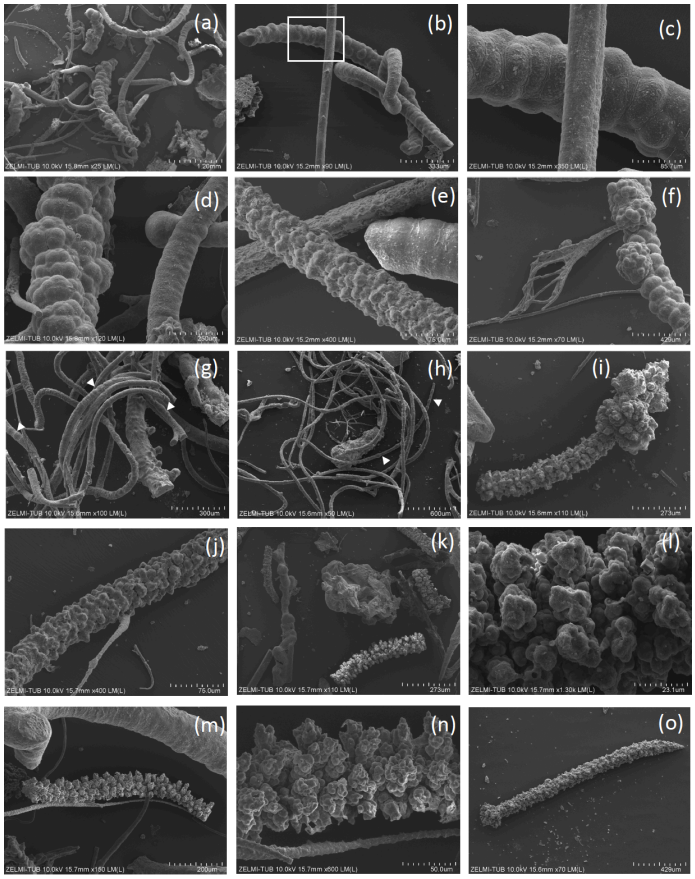


**Fig. 6 SEM images of filaments with structured, rough surface 2. (a) Overview illustrating joint occurrence of smooth, slightly, and strongly bulbous surfaces (sample #5). (b) Joint occurrence of straight, slightly and strongly curved filaments; rectangle indicates detail in (c) with irregular segmentation of the slightly curved filament. The straight filament also shows a slight structure on the surface (lower right). (d) Joint occurrence of slightly bulbous (right) and strongly bulbous filaments, transitional to outgrowths. (e) Filament with indication for segmentation (right) and filament with strongly sculptured surface; note small diameter (75 µm) compared to the large filament in (d). (f) Thick filament with bulbous outgrowths, next to thin agglutinated filaments. (g, h) Thin filaments with indication for segmentation (white triangles). (i) Complete filament of approximately 1 mm length with strongly sculptured surface and outgrowths. (j) Part of a filament with strongly sculptured surface. (k) Joint occurrence of filaments with strongly sculptured surface and smooth surface, together with and irregularly shaped object (center). (l) Detail of strongly sculptured surface, which consists of small ball-shaped outgrowths. Note fluorite crystal in upper right, below label (m), which shows joint occurrence of thick filament (top) with slight striation perpendicular to filament length, and filament with strong sculptured surface, detail shown in (n). (o) Almost 2 mm long complete filament, one thin end, one with outgrowths.**

293

294 **4.1.2 Hollow objects**

295 Some objects appear hollow (Fig. 7); one object (Fig. 7a, b) has a hollow lower part transitional
296 into a more solid upper, strongly bulbous part. The hollow rather irregular objects (Fig. 7c)
297 occur together with filaments. Filaments can be also hollow (Fig. 7d-h) and the thickness of the
298 outer rim is approximately 2 µm (Fig. 7h). This is the width of the fossilized outer part of
299 filaments, which we documented in the previous study (Franz et al., 2022a) and therefore we
300 interpret the hollow objects as organisms in which the interior part was completely decayed
301 during and after the fossilization process. Some of the hollow objects are bowl-shaped (Fig. 7i-
302 n). One such object (Fig. 8) is >1 mm large and from the view in different perspectives is can
303 be seen that it is grown onto mineral substrate; next to the clay minerals fluorite is a
304 characteristic mineral and indicates a high fluorine activity in the fossilizing fluid (Franz et al.,
305 2022a). The base of mineral substrate is followed by an approximately 10 µm thick solid rim
306 with bulbous outgrowths.

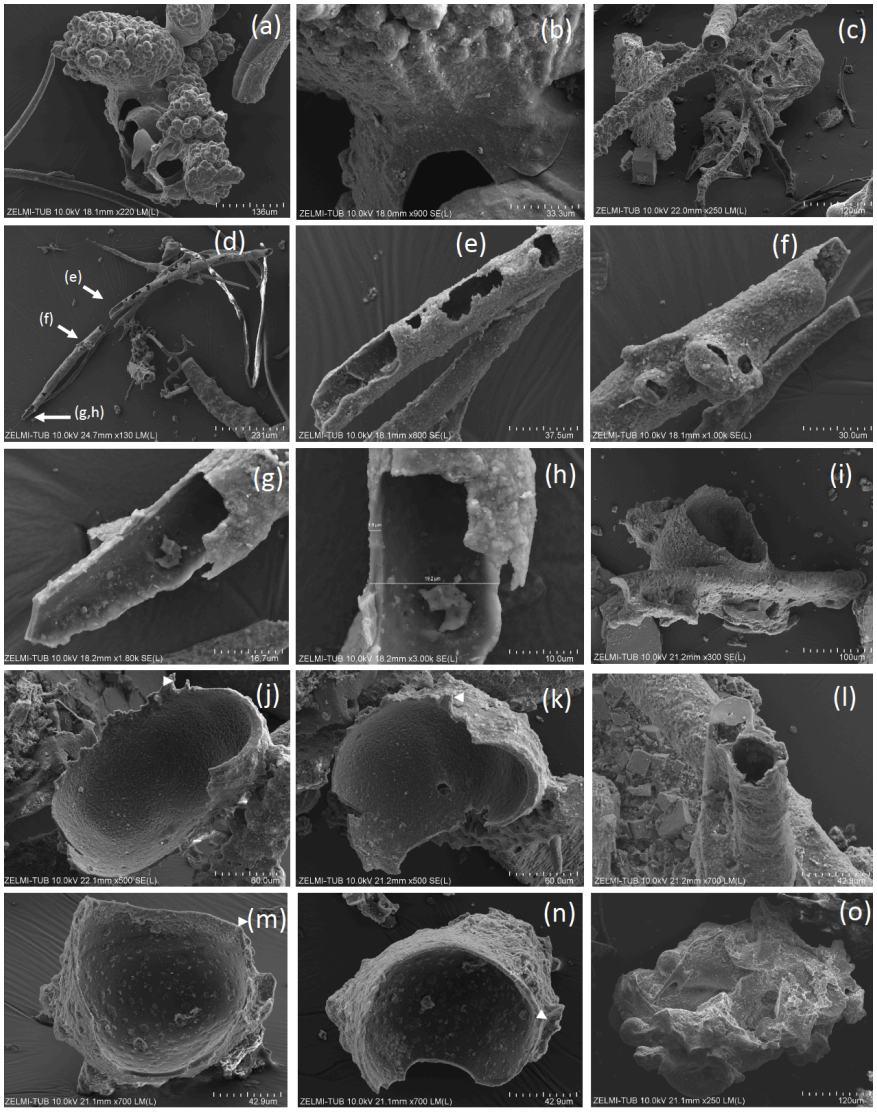


**Fig. 7 SEM images of hollow objects. (a) Irregular-bulbous base of a strongly sculptured object, with (b) detail of the transition (center in (a); sample #5). (c) Irregular hollow object below filaments (sample #6). (d) Hollow filament, approximately 1 mm preserved length; position of enlarged parts in (e-h) is indicated (sample #5). The mineralized rim is 1-2 µm wide, diameter near 20 µm. (f) Bulbous outgrowths are also hollow. (i) Filament with an attached hollow form, similar to outgrowths, but much larger (sample #6). (j, k) Same object as in (i), enlarged in two different perspectives; white triangle indicates identical point. (l) Hollow filament next to a filament with a central channel (sample #6). (m, n) Isolated hollow bowl-shaped object in two different perspectives; white triangle indicates identical point (sample #6). (o) Irregular object, partly hollow (sample #6).**

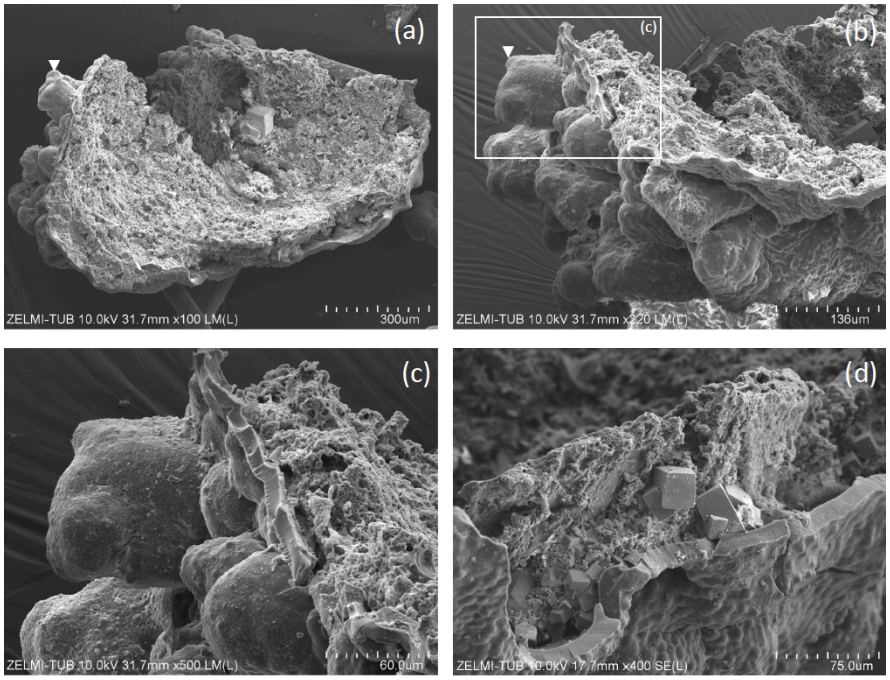


**Fig. 8 SEM images of >1 mm large bowl-shaped object (sample #5) (a) seen from below, grown onto mineral substrate; euhedral crystal is fluorite, white triangle indicates position of (b), enlarged part of the rim. Rectangle indicates position of (c) illustrating the base of mineral substrate (right) followed by an approximately 10 µm thick solid rim with bulbous outgrowths. (d) Detail of the solid rim with several fluorite crystals.**

### 4.1.3 Spherical objects

Most spherical objects (Fig. 9) appear as rather complete, with only some parts broken off. One object with a double-ball shape (Fig. 9a,b) is clearly grown onto the substrate (Fig. 9c). The double-ball with remnants of a sheath points to cell separation. Note the different size of the objects from < 10 µm (Fig. 9m) to > 1 mm (Fig. 9g). Two small objects identified on the etched beryl surface appear like seeds or spores (Fig. 9l, m).

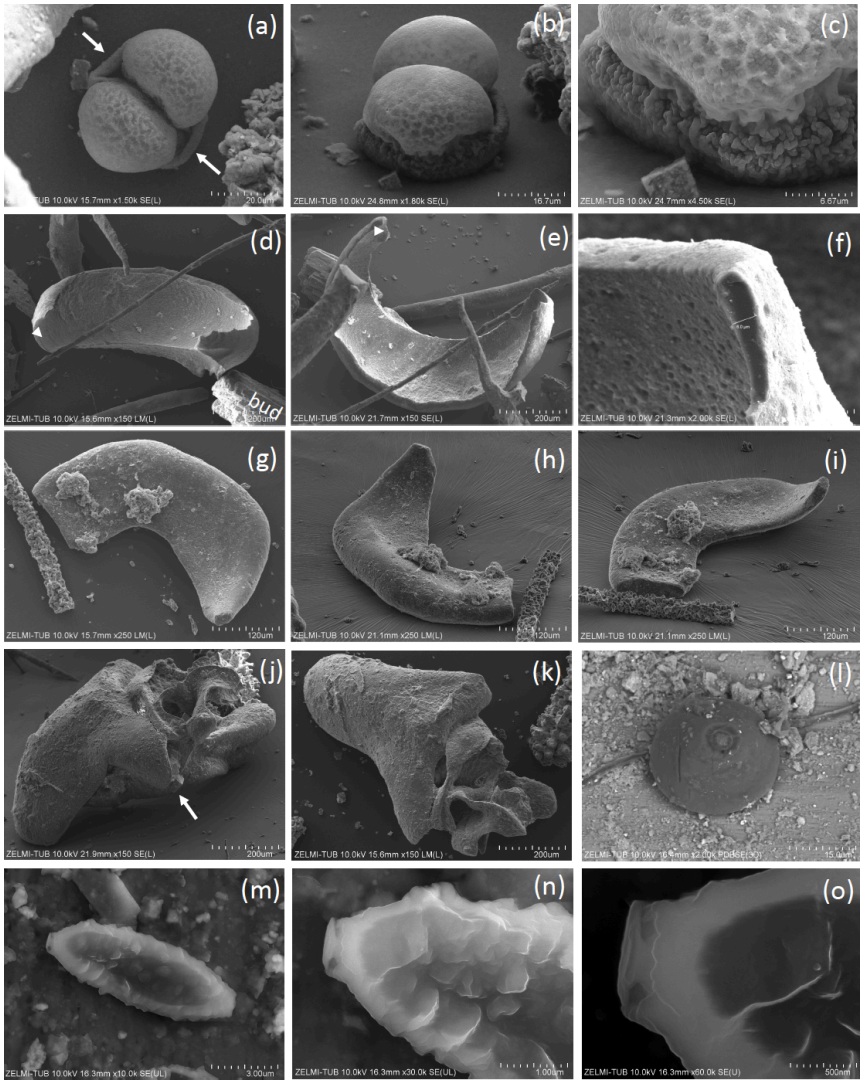


**Fig. 9 SEM images of spherical objects. (a, b, c) Same object in different perspective and magnification; arrows in (a) point to a sheath; the euhedral crystal in (c) is fluorite. The object growth from a flat mineral surface into a double-ball with dented surface. (d, e) Same object in different orientation; white triangle indicates identical position; bud = buddingtonite. (c) The thickness measured at one point is approximately 6 µm. (g, h, i) Approximately 0.5 mm large object in different perspective with mineral incrustations. (j, k) Irregular, partly hollow object in different perspective. (l) Perfectly round object, sitting on a filament, on etched surface of beryl (compare Fig. 2d); the circular round structure on its top is beam damage. (m, n, o) Oval object on etched surface on beryl (compare Fig. 2i). The lower contrast (dark) in the central part indicates less dense (partly hollow) material.**

345 **4.1.4 Irregular objects**

346 Irregular, flaky objects are abundant, especially on the surface of the beryl crystal (Fig. 2e, f),
347 but also in many samples (e.g. Fig. 6k, 7a, c, o, 8, 9j, k). They show the same fossilization
348 features as the filaments with a thin rim enriched in Si, Al, Ca, and P, loss of N, and oxygenation
349 (Franz et al., 2022a). In some samples (Fig. 6f) filaments appear agglutinated by OM and we
350 interpret these as well as the irregular objects on the beryl crystals as fossilized biofilm.

351 4.2 Internal structure

352 For investigation of the internal structure we used SEM images of broken filaments and other
353 objects, as well as polished sections embedded in epoxy, investigated by BSE images including
354 mapping of element distribution. Data of open-pyrolysis and TEM data (Franz et al., 2022a)
355 had shown that the OM is highly mature, amorphous oxy-kerite. Indications for an outer cell
356 wall are absent, because the outer rim of the fossils is silicified, partly with formation of mineral
357 incrustations.

358 Segmentation of filaments, which might be a characteristic phenomenon for certain organisms
359 and is observed in the filaments' morphology (Figs. 5g, h, 6b, c, e, h) is not obvious in cross
360 section, but one section shows internal cracks, separating the filament in ~50 µm to 100 µm
361 wide segments (Fig. 10a, b). A section of a bulbous fossil shows cracks, which separate the
362 individual bulbs from each other (Fig. 10g, h).

363 The outer rim of the filament shows the typical enrichment of Si and Al (Fig. 10b), and the
364 inner, homogenous and not silicified part shows abundant, nm-sized mineral inclusions (Fig.
365 10c). They are located in the central part and thus not related to the fossilization process,
366 irregularly distributed or in linear array of several crystals (Fig. 10e, h). The minerals were
367 analyzed with the EDS-system and due to their small size in the order of a few nanometers,

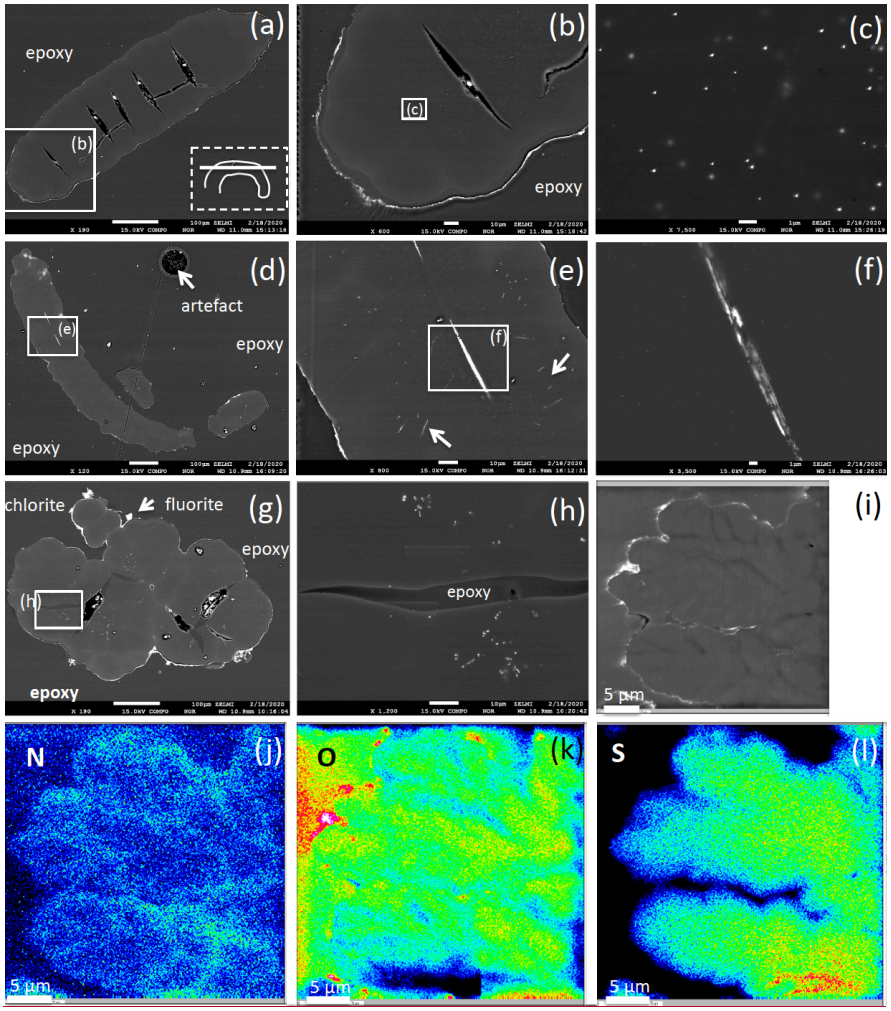


Gelöscht:

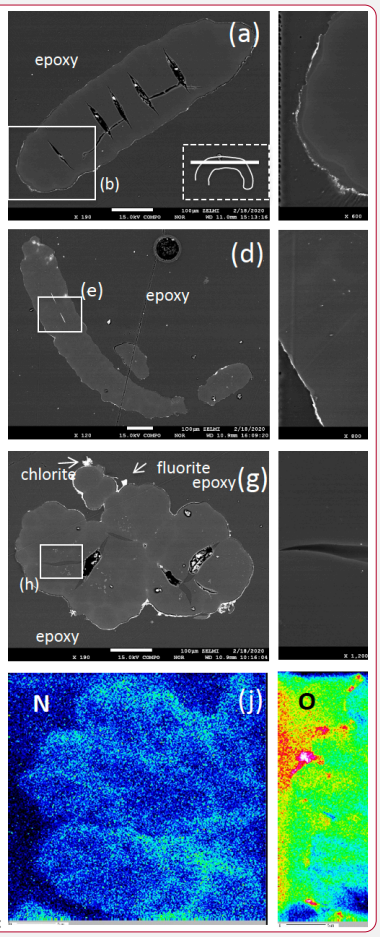


**Fig. 10: BSE images of filamentous (a-f) and bulbous fossils (g, h, i), embedded in epoxy, polished thin section and element distribution (j, k, l). (a) Part of curved filament; orientation of section is shown in rectangle (dashed lines), position of enlargement (b) in rectangle (solid lines). Open cracks (black contrast, with impurities from polishing material) indicate approximately 50 µm to 100 µm wide segments. (b) Silicified outer rim (white contrast, irregular) and a narrow, up to 10 µm wide inner rim, are interpreted as effect of fossilization. The homogeneous appearing central part shows in the enlarged image (c) irregularly distributed inclusions, tens of nm in size, of Bi-S-Te minerals. (d) Filament with two, central oriented Bi-S-Te mineral inclusions, approximately 50 µm in length and 1-2 µm wide, enlarged shown in (e) and (f). Arrows in (e) point to straight aligned inclusions, and (f) shows irregular contrast, possibly caused by heterogeneous distribution of Fe and Cu in the Bi-S-Te minerals. (g) Bulbous fossil, with silicified rim**

**and encrustations of chlorite and fluorite. Cracks, partly filled with epoxy, separate individual bulbs from each other. (h) Enlarged part showing irregularly distributed and aligned nm-sized Bi-S-Te mineral inclusions, and epoxy-filled crack. (i) Bulbous fossil with element distribution of N (j), O (k), and S (l), indicating an interior structure with possible former cell walls. The color code goes from cold to warm, blue = low concentration, red = high concentration.**

much smaller than the excitation volume of the electron beam, only mixed analyses with the organic material could be obtained (Table 2). Recalculation of the analyses without the organic compounds C, O, and N yielded an atomic ratio of Bi:(S,Te) near 1:1, indicating minerals such as ingodite Bi(S,Te) or joseite $Bi_4(S,Te)_3$.The example of the bulbous filament (Fig. 10g) with inclusions also shows a Bi(S,Te) mineral, located in the central part. The heterogenous BSE contrast is caused by different trace compounds of Fe and Cu. Element distribution of N and O (Fig., 10j, k) in a bulbous fossil, indicated by different BSE contrast (Fig. 10i), show an internal structure, possibly indicating a primary separation into different cells, whereas S (Fig. 10l) shows a systematic decrease towards the rims of the object, as a result of decay and/or fossilization.

Table 2 EDS analyses of Bi-sulfide-telluride inclusions

| **Analysis#** | **15 06[1]** | **13 03[2]** | **13[3] n=18** | **Min-max** |
|---|---|---|---|---|
| S atom% | 0.27 | 2.59 | 0.20 | n.d. – 0.52 |
| Te | 0.13 | 0.06 | 0.12 | n.d. – 0.51 |
| Bi | 0.29 | 2.05 | 0.24 | 0.01-0.68 |
| Pb | 0.03 | n.d. | n.d. | |
| Fe | n.d. | 0.19 | n.d. | |
| Cu | n.d. | 0.22 | n.d. | |
| C | 86.24 | 84.86 | 83.38 | 80.19-96.15 |
| N | 5.91 | 4.89 | 3.16 | n.d.-7.18 |
| O | 7.13 | 5.14 | 10.12 | 2.74-15.78 |
| Sum[4] | 100 | 100 | 100 | |
| recalculated | 15 06 | 13 03 | 13 n=19 | Min-max |
| S atom% | 38 | 51 | 37 | 3-55 |
| Te | 18 | 1 | 25 | 1-90 |
| Bi | 40 | 40 | 46 | 7-68 |
| Pb | 4 | 0 | | |
| Fe | | 4 | | |
| Cu | | 4 | | |
| Sum | 100 | 100 | 100 | |

[1] Fig. 10h; [2] Fig. 10f inclusion in channel; [3] average of 18 analyses, inclusions in matrix, Fig. 10b,c; [4] normalized; n.d. = not detected

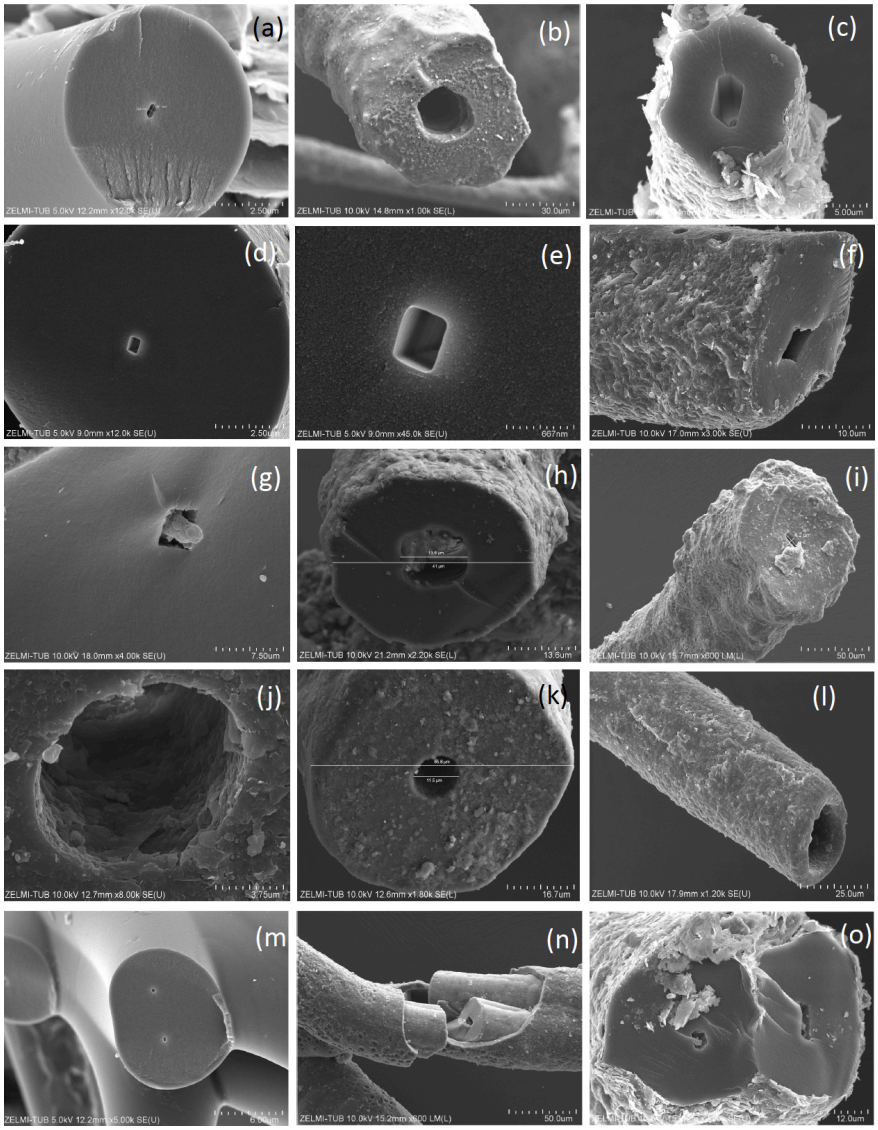


**Fig. 11: SEM images of broken filamentous fossils, illustrating the central channel. (a,b,c) Six-sided channel in filament with (a) smooth outer surface, (b) dented surface, and (c) strongly mineralized surface. (d, e, f, g) Rectangular channel; (e) is enlarged part of (f). (h) Round, slightly irregular channel. (i) 4 µm x 6 µm wide channel on filament with dented surface. (j) Round channel, enlarged from (k), approximately 12 µm wide in a filament of nearly 70 µm diameter. (l) Slightly conical end of a filament with large, round channel. (m) Two filaments one with a small µm-wide channel attached to a hollow**

**filament. (n) Channel in a filament with sheath-like structure. (o) Two filaments with six-sided channels.**

A very characteristic feature of the filaments is a central channel (Fig. 11), observed in many but not all of the filaments. The cross section of the channel can be six-sided (Fig. 11a-c,m), rectangular (Fig. 11d-f), or round (Fig. 11h-l). The channel diameter is variable and ranges from approximately 0.5 µm to 25 µm in filaments with an outer diameter between approximately 5 µm and 100 µm; examples in Fig. 11 show 5 µm with a channel of 260 nm x 550 nm (a), 50 µm with a channel of approximately 20 µm (b), 10 µm with a channel of 2.5 µm x 4 µm (c), 100 µm with a channel of 400 nm x 560 nm (d,e), 41µm with a channel of 14 µm (i).

4.3 Stable isotopes and C/N variation

Stable isotopes of C and N were obtained from all bulk samples (Table 1); it was not possible to determine individual fossilized objects. In addition, we determined OM in black opal and OM adherent to topaz (see sample list in Franz et al., 2022a).

Results of $\delta^{13}C$ and $\delta^{15}N$-determination and the molar C/N show a large variation (Fig. 12). All $\delta^{13}C$ values are negative, and for kerite fossils vary between -47 (sample 2) and -31 ‰ (sample 1); $\delta^{15}N$ values vary between ~3 to 4 ‰ (samples kerite 0, 4) and ~10 ‰ (samples 1, 3). OM associated with opal and topaz (considered as 'secondary') and buddingtonite, which obtained its N from decayed OM, is less negative and homogeneous in $\delta^{13}C$ with values between -25 and -27 ‰. The C-values should be considered as maximum values, since alteration either by deep-seated $CO_2$ from the mafic magmas or from meteoric waters would have increased $\delta^{13}C$. The close group of $\delta^{13}C$ and $\delta^{15}N$ values for secondary OM indicates that during maturation and decay they all have reached a similar value. The variation of the N-isotopes is not correlated with the C-isotopes, and there is also no correlation with C/N.

Table 3 Results of $\delta^{15}N$, $\delta^{13}C$, and molar C/N of bulk kerite samples

| Sample# | weight mg | $\delta^{15}N$ ‰ | mg N/sample | % N | $\delta^{13}C$ ‰ | mg C/sample | % C | molar C/N |
|---|---|---|---|---|---|---|---|---|
| 1 | 2.76 | 9.99 | 0.038 | 1.37 | -30.66 | 1.91 | 69.07 | 58.74 |
| 2 | 2.37 | 8.44 | 0.067 | 2.85 | -46.99 | 0.63 | 26.52 | 10.87 |
| 3 | 2.21 | 10.23 | 0.027 | 1.20 | -31.38 | 1.24 | 56.10 | 54.58 |
| 4 | 2.52 | 2.98 | 0.033 | 1.31 | -33.61 | 0.44 | 17.34 | 15.48 |
| 5 | 4.01 | 7.37 | 0.096 | 2.38 | -45.19 | 0.88 | 21.98 | 10.78 |
| 6 | 3.14 | 7.79 | 0.037 | 1.19 | -44.06 | 0.27 | 8.55 | 8.39 |
| 7 | 4.29 | 6.87 | 0.074 | 1.73 | -43.58 | 0.71 | 16.54 | 11.17 |
| Opal 8 | 50.15 | 2.02 | 0.013 | 0.03 | -25.32 | 0.55 | 1.09 | 49.23 |
| Topaz 9 | 54.46 | 1.56 | 0.023 | 0.04 | -25.73 | 0.38 | 0.69 | 18.89 |

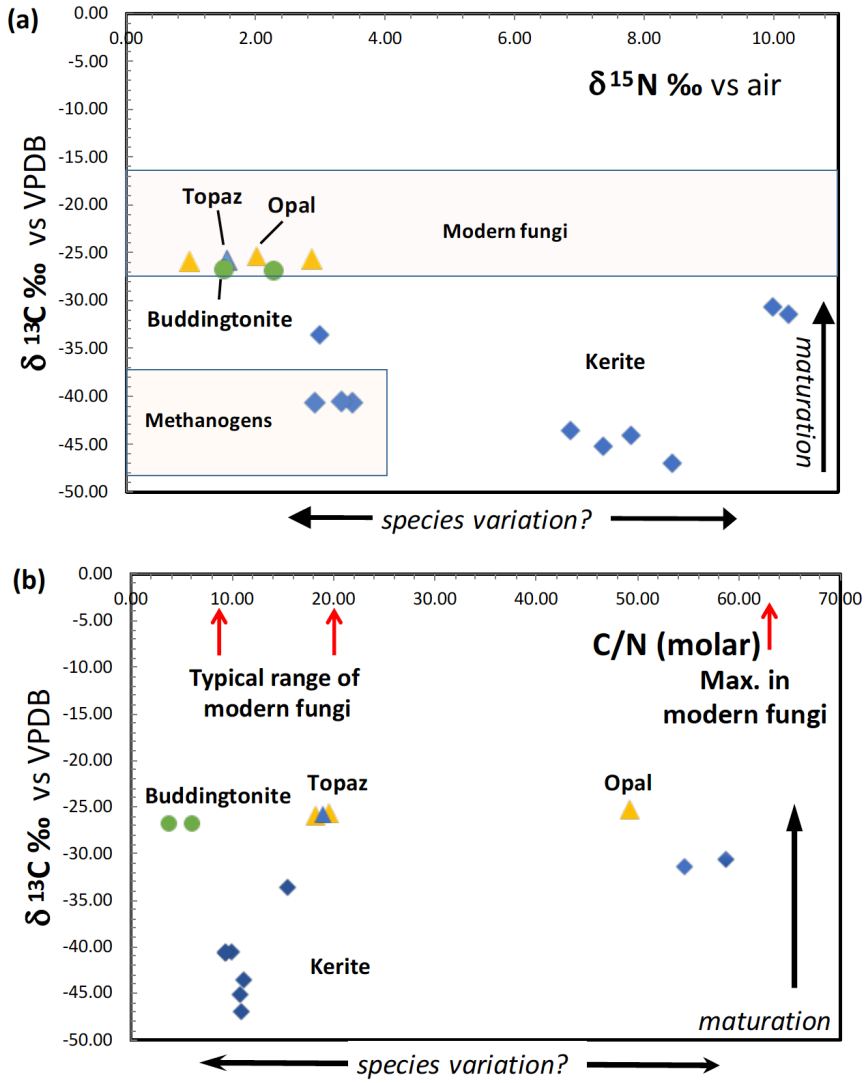


**Fig. 12: (a) Results of determination of $\delta^{13}C$ and $\delta^{15}N$ of Volyn biota and degraded kerite. Symbols: Blue diamonds – dominantly filamentous kerite, with small amounts of flaky and spherical OM; yellow triangle - black opal with OM; blue triangle - OM adherent to topaz; green dots - buddingtonite from breccia (from Franz et al., 2017). Fields of modern fungi from Mayor et al. (2009) and methanogens are summarized in Struck (2012). (b) Molar C/N ratio of kerite fossils and degraded OM. Range of C/N of modern fungi from Mayor et al. (2009).**

## 4.4 FTIR investigation

All measured FTIR spectra of morphologically different kerite fragments in the sample #0 are very similar (Fig 13a) and resemble closely the chitosan spectrum (Fig 13b); both spectra are dominated by two main groups of absorption bands located in the regions of 3500-2500 $cm^{-1}$ and 1800-900 $cm^{-1}$. The first group consist of overlapping broad bands due to O-H and N-H stretching vibrations, with a group of characteristic narrow peaks of C-H stretching vibrations on their long-wavelength wing in the region of 2960-2870 $cm^{-1}$ (Fig. 13; for detailed band assignments and for spectra of chitin see Table 1 Supplement). The peak in vicinity of 1650 $cm^{-1}$ is diagnostic of C=O group (Wanjun et al., 2005; Coates, 2011; Loron et al., 2019), the band at 1560 $cm^{-1}$ (broad shoulder near 1570 $cm^{-1}$ in kerite spectra) was assigned to N-H

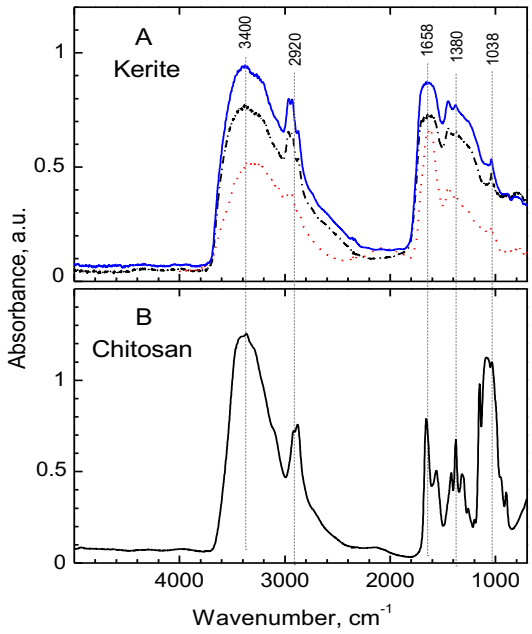


**Fig. 13: FTIR spectra of filamentous fossil compared to standard materials chitin and chitosan. (a) Complete spectra of three pieces of sample kerite #0, the sample with less mineralization, showing two main regions of absorption: 3500 $cm^{-1}$ to 2800 $cm^{-1}$ and 1850 $cm^{-1}$ to 900 $cm^{-1}$; (b) Standard material chitosan. Compared to chitosan the major absorption bands in kerite spectra are broader, the weak shoulder near 3100 $cm^{-1}$ in chitosan spectrum is not present in kerite. The narrow triplet near 2950 $cm^{-1}$ is observed as doublet in chitosan, shifted to lower wavenumbers. In the part from 1800 $cm^{-1}$ to 700 $cm^{-1}$, kerite shows only broad absorption, shifted towards higher wavenumbers compared**

**to chitosan, with three superimposed distinct weak peaks at 1450 cm$^{-1}$, 1380 and 1038 cm$^{-1}$; the first is not present in chitosan, which has a number of distinct peaks in this region.**

bending vibrations in amide group. The relatively weak band near 1420 cm$^{-1}$ (1450 cm$^{-1}$ in kerite) was attributed to C-H bend (Loron et al., 2019), and the sharp peak at 1380 cm$^{-1}$, which was reported in cellulose, chitosan, and chitin spectra, was assigned to superposition of O-H bend (pyranose ring; Li et al., 2009) and symmetrical bend of $CH_3$ group. A band centered near 1315 cm$^{-1}$ in chitin and chitosan spectra due to C-N stretching vibrations in amide group (Vasilev et al., 2019; Wanjun et al., 2005) is not observed in kerite.

A broad, weak band at around 2100 cm$^{-1}$ is present in spectra of kerite and chitosan (Fig. 13), and the same type of weak bands are shown in published chitosan spectra (see Table 1 Supplement), but not mentioned and assigned. It can probably be attributed to overtone or combination bands of pyranose ring vibrations. At lower wavenumbers, in all measured spectra there is a series of strong (1150, 1180, 1030 cm$^{-1}$) and several weak bands caused by different types of C-O vibrations in polysaccharides (Nakamoto, 1997; Wanjun et al., 2005; Li et al., 2009; Coates, 2011; Loron et al., 2019; Vasilev et al., 2019).

A general observation is that in kerite spectra, compared to chitosan, all characteristic absorption bands of the amide group and the pyranose ring become broader and weaker, in agreement with earlier studies of spectroscopic changes during chitin/chitosan degradation (Wanjun et al., 2005; Zawadzki and Kaczmarek; 2010; Vasilev et al., 2019). Nevertheless, the main absorption features caused by amide group, diagnostic of chitosan, are still present in kerite spectra.

## 5 Discussion

### 5.1 Interpretation of morphological and internal characteristics

The Volyn biota show an astonishingly large variation of different types of filaments and other forms, pointing to the interpretation that different organisms were involved. We have already interpreted the flaky objects of OM on the surface of beryl crystals (Fig. 2e,f) as biofilms (Franz et al., 2022a). Agglutinated filaments (Fig. 6f) and the hollow object agglutinated to a filament (Fig. 7i) can similarly be interpreted as fossilized biofilms. The sheath-structure (obvious e.g. in Fig. 5i, j) is also an indication for the presence of a biofilm or extracellular polymeric substances (EPS).

Some objects have a base onto which they grew (Figs. 3j-l, 8, 9a-c) and one object shows a hollow lower part, from which bulbous outgrowths originate (Fig. 7a, b), pointing to sessile organisms. Filaments are generally fragmented, but a few filaments have been found with two intact ends (Figs. 4c, g, 6i, o), and we interpret this as non-sessile, free-living organisms.

Thickness of the filaments varies from ≤10 µm to >200 µm. In filaments with diameter up to approximately 30 µm, branching with thinning out of the branch clearly show that these are within-species variations (irregular diameters of filaments, Fig. 2i, j, are interpreted as collapse structures during fossilization). However, very thick filaments with diameters in the range of ≥200 µm with a structured, bulbous surface (e.g. Fig. 6), or conical objects (Fig. 4m) are interpreted as different species. The length of both types of filaments reaches the mm-range, and since they are fragments possibly up to cm-length.

Branching as indication for growth of the organisms is typical in the thin filaments, with Y-, T-, double-T-, and multiple branching (Fig. 3), but anastomosing was not observed. In thick filaments with diameter near 200 µm branching was not found. The ends of filaments also hint to the type of growth. Simple round ends are rare, more typical are ball-shaped ends (Fig. 4). Ball-shaped outgrowths along filaments are interpreted as beginning of a branching (Fig. 4h). In the complete filaments (Fig. 4c, g) with one end thinning out, one with a ball-shaped end, the thinning-out end is possibly the origin, the ball-shaped protrusions the growing end, because ball-shaped ends are rather continuous in shape, from a small protrusion (Fig. 4b) to a more complete ball (Fig. 4f, i). Similar protrusions were found at the end of recent, large bacterial filaments (Volland et al., 2022). However, branched, thinning-out ends of the filaments (Fig. 3j-l, m) indicate ends similar to Spitzenkörper, what in modern fungi is described as a continuous and indefinite process of cell extension (Fischer et al., 2008).

Segmentation in thin filaments (Figs. 5m, 6g, h) with distances of a few µm up to tens of µm is accentuated by mineralization (Fig. 5n), with irregular ridges caused by mineralization. Thick filaments do not show a clear segmentation; the morphology is more irregular and shows rounded, polygonal structures on the surface with dimensions of approximately 20-30 µm (parallel to filament axis) x 35-70 µm (perpendicular to filament axis) (Figs. 5g, h, i, 6b, c). Between the polygonal structures on the surface, remnants of a sheath are visible. In cross section (Fig. 10) segmentation is clearly visible by cracks with a distance of approximately 50-100 µm.

Bulbous forms (Figs. 7a, b, 8) mark the beginning of growth of some objects, and bulbous outgrowths are very typical for thick filaments (Fig. 6, d, f), which extend into approximately

**Gelöscht:** planktonic

**Gelöscht:** , or organisms which grew in a soft (possibly organic or clay mineral) substrate

**Gelöscht:** s

20 µm large objects, which consist of smaller bulbs (Fig. 6l, n). In thin filaments with typical branching, the outgrowths are rare and more regularly ball-shaped (Figs. 3f, g, 4h), indicating one species with prominent growth by branching of thin filaments, and another species with growth by outgrowths along thick filaments.

Among the spherical objects, only the small ones with a size of a few µm (Fig. 9l-o) resemble spores or other types of seeds/fruit bodies. The irregular, large objects several hundred µm in size (Fig. 9d-k) do not fit into any scheme of known organisms. Similarly, there is no obvious interpretation for the large bowl-shaped and irregular hollow objects (Fig. 8). The small double-object with a partly preserved sheath (Fig. 9a-c) grown on a substrate has some similarities with cell division.

Gelöscht: (micro)

The function of the conspicuous central channel (Fig. 11) in many, but not all filaments with different shape in cross section is speculative, likely providing pathways for transport of components for cell extension along the filament axis. In one example we observed a type of filling in the channel (Fig. 11g), so in the original organisms it might have been filled with an easily degradable substance. It is not clear if a hollow form (Fig. 7e, l) is a different phenomenon or due to special preservation conditions. The width of the preserved rim is in the same order of magnitude as the silicified rim (1-2 µm) and therefore it might just be a remnant of a filament, in which the central part was completely degraded.

Another special feature of the internal structure are the nanometer-sized mineral inclusions of Bi-S-Te minerals (Fig. 7). The organisms were able to concentrate these elements, either irregularly distributed (Fig. 7c) or rod-like aligned (in a bulbous object; Fig. 7h) or within the channel (Fig. 7e). It is unclear if the relatively large Bi-S mineral with some Cu and Fe contents in the center of a thick filament in the central channel is the original position of the Bi-S concentration or an effect of fossilization. Modern fungi are able to concentrate Te (and Se) as nm-sized crystals (Liang et al., 2020) and could be used in technology for soil mycoremediation (Liang et al., 2019). In black shales, the organophilic element Bi might behave similar as Se (Budyak and Brukhanova, 2012). Biogeochemistry of Te is probably analogous to Se (Missen et al., 2020), but little is known about the link of Bi to S and Te in OM (such as in coal, e.g. Finkelman et al., 2019). The concentration of Bi-S-Te in the organisms of the Volyn biota is another indication for fungi-like organisms, although other organisms such as bacteria are also able to concentrate Te (Missen et al., 2020).

Remnants of cell membranes, separating individual cells, could not be identified, and to answer the question if some of the organisms were multicellular is speculative. However, the large size

of many objects of the Volyn biota already indicates that possibly they were not single-celled but multicellular, notwithstanding that single-cell bacteria (*Thiomargarita magnifica*; Volland et al., 2022) can reach the size of cm. These macroscopic single-cell bacteria show a very simple straight filament, whereas the large objects from the Volyn biota show a much more complicated form; the surface of large filaments shows a bulbous structure with sizes in the order of tens of µm (Figs. 5g-i, 6c, f, 9a, b), well visible with a polygonal network (Fig. 5j). In the internal structure we also see phenomena that could be explained as separate cells, such as the gaps in a filament (Fig. 10a) or in a bulbous object (Fig. 10g). The interior structure visible in the element distribution of N (Fig. 7j) might indicate the original distribution in former interior cell walls, in which chitin-like substance was concentrated. Finally, the small spherical object shown in Fig. 9a, b might be taken as two cells, with an envelope of a sheath.

**5.2 Stable isotopes**

Modern fungi show a very wide variation of $\delta^{15}N$ from -5 ‰ to +25 ‰, with the main cluster between - 5 ‰ and +12 ‰, and $\delta^{13}C$ is restricted to -19 ‰ to -29 ‰ $\delta^{13}C$, with the main cluster at -22 ‰ to - 28 ‰ $\delta^{13}C$ (Mayor et al., 2009; Fig. 12a). Whereas the N-isotopic signature of kerite is consistent with the interpretation as fossil fungi, the C-isotopic signature is much lower than that of modern fungi. However, fungi live from consumption of organic matter, and the C-isotopic signature is then transferred to the fungi without strong isotopic effect (Peterson and Fry, 1987). I. e. during incorporation of carbon from modern plants to fungi, the $\delta^{13}C$-signature of -27 ‰ to -30 ‰ in plants changes to - 25 ‰ to -27.5 ‰ $\delta^{13}C$ in fungi (e.g. Högberg et al., 1999). Assuming that the isotope fractionation in the Volyn biota was similar, the consumed organism had a C-isotopic signature of c. -35 ‰ to -50 ‰ $\delta^{13}C$. These very low values are consistent with the interpretation that the primary organisms were methanogens. Another factor, which must be considered, is intracellular heterogeneity as observed in bacteria (Lepot et al., 2013). The membrane (lipids) can have a signature of 10 ‰ $\delta^{13}C$ lower than the bulk cell, and degradation during fossilization of the proteins and polysaccharides can lower the now determined C-signature. It is also possible that the fungi consumed biofilm. Fossil biofilms of the 2.75 Ga Hardey Formation (Australia), probably coexisting with methanogens, methanotrophs, and sulfur-metabolizing bacteria have $\delta^{13}C$ of -55 ‰ to -43 ‰ (Rasmussen et al., 2009), well in the range of $\delta^{13}C$-values observed here. The biofilms, described by Rasmussen et al. (2009), lived in synsedimentary cavities similar to stromatolites, pointing to

603 the importance of cavities for the preservation of organic matter, similarly as the biofilms at
604 Volyn in the deep biosphere.

605 Maturation clearly affects the C- and N-isotope ratios, which we see in degraded OM preserved
606 in black opal, in OM adherent to topaz, and buddingtonite which obtained its $NH_4$ from OM.
607 These samples have much more positive $\delta^{13}C$ values around -26 ‰ and more homogeneous
608 $\delta^{15}N$ values near +1.5 to +3 ‰ (Fig. 12a). In contrast, the large variation of $\delta^{15}N$ between 3 ‰
609 and 10 ‰ in the kerite samples (Fig. 12a) and C/N between 10 and >50 (Fig. 12b) possibly
610 indicates a variation of the species. These values were less influenced by maturation, as there
611 is no correlation between $\delta^{13}C$ and C/N in all samples (fossils and degraded OM). Alleon et al.
612 (2018) in their description of the 3.4 Ga old Strelley Pool microfossils (Western Australia)
613 argued that though the fossils experienced heating up to 300 °C, the C/N did not change
614 significantly. Also, for anthracite coal it has been shown that the original C/N did not vary with
615 coalification (Anwita et al., 2020).

616 Loron et al. (2019) reported fossil fungi from the 1 Ga Grassy Bay Fm Canada, and provided
617 proof via chitin remnants (FTIR) and showing the characteristic bilayered fungal cell walls
618 (TEM data). However, the few SEM images for the Grassy Bay biota do not allow a comparison
619 with the Volyn biota. Following their discussion, the FTIR investigation of the filamentous
620 Volyn sample shows good indications for preserved chitosan as part of the OM. Degradation
621 studies of chitosan (Wanjun et al., 2005; Zawadzki and Kaczmarek; 2010; Vasilev et al., 2019)
622 showed that the spectra of kerite has the same characteristic bands as chitosan at approximately
623 250 °C; at lower as well as at higher temperatures these bands disappear. Completely
624 independent temperature estimates for the fossilization based on phase equilibria of Be minerals
625 yielded the same temperature range (Franz et al., 2017).

626 **5.3 Taxonomy and comparison with Precambrian biota**

627 Film-like microfossils were described from the 3.4 Ga old Strelley Pool (Western Australia;
628 Alleon et al., 2018), the 3.3-3.5 Ga old Onverwacht Group (Australia; Westall et al., 2001),
629 from the 2.75 Ga old Hardey Formation (Australia; Rasmussen et al., 2009) and there is little
630 doubt that biofilms existed for a long time in the Earth's history and are an integral component
631 of the ancient life cyle (Hall-Stoodley et al., 2004). It seems safe to assume that the irregular
632 (Fig. 2f, and images in Franz et al., 2022a) and sheath-like structures (Figs. 5i,j, 6f, 9a) of the
633 Volyn biota were biofilms.

634 We have already pointed out that some of the organisms show analogies to fungi. Based on the
635 molecular clock technique, Wang et al. (1999) estimated the divergence between the three-way

split of the animal-plant-fungi kingdoms at 1.58±9 Ma, much earlier than the 'Precambrian explosion'. This age is in the same range as the minimum age of the Volyn biota. Other molecular clock estimates indicate that the first zygomycetous fungi occurred on Earth during the Precambrian, approximately 1.2–1.4 Ga ago (review in Krings et al., 2013). Diversification of fungi and transition to land was dated at ca. 720 Ma (Lutzoni et al., 2018) and they estimate the origin of fungi at ca. 1240 Ma, similarly as Berbee et al. (2020), who placed the origin of fungi at ca. 1300 Ma. If indeed the Volyn biota contain fungi-like organisms, their origin as well as colonization of land occurred earlier than ca. 1500 Ma.

Bengtson et al. (2017) reported fungus-like organisms in the 2.4 Ga Ongeluk Formation (South Africa) from the deep biosphere, which are however not terrestrial but marine. The important fact is that these fossils were found also in open cavities, though of a completely different size, mm-amygdales in low-grade metamorphic basalt, in contrast to the huge cavities of tens of meter size in the pegmatites from Volyn. The filaments from the Ongeluk biota with a diameter of ca. 2 µm to 12 µm are generally thinner than the Volyn biota and show anastomosis, but also Y- and T-branching, and sometimes bulbous protrusions, 5-10 µm in diameter. A special feature is what Bengtson et al. (2017) call 'broom structure', diverging filaments growing from a substrate of clay minerals (chlorite), and the filaments consist also of the same type of chlorite. These structures (shown in 2D in thin sections) could be similar as the object from the Volyn biota (Fig. 3j, k, l), and what we called 'multiple branching' (Fig. 3c, e, g). A significant difference between the two biota is the fossilization process, which resulted in the Ongeluk biota in complete replacement of the filaments by clay minerals, whereas at Volyn fossilization is restricted to the outermost rim and most of the C is preserved (Franz et al., 2022a).

Good evidence for fungi-like organisms were reported from the early Ediacaran Doushantuo biota, at approximately 635 Ma (Gan et al., 2021). These fossils are pyritized, but with remnants of organic matter, and consist of branching filaments (Y-, T-branching, but also with A- and H-type and anastomosis) and associated hollow spheres. Compared to the Volyn biota, the filaments are thinner (two types, one with average 6.8 µm, one with average 2.7 µm), whereas the observable length in thin section with hundreds of µm is possibly in the same range as in the Volyn biota. The spheres of the Doushantuo biota are hollow and coaxially aligned, but also similar to what we described as ball-shaped outgrowths; their size varies from average 16 µm to 20 µm in small ones and large spheres with 36 µm to 102 µm, similarly to the Volyn biota (Fig. 4h, i for the small spheres, Fig. 4j for large spheres). The fact that the spheres of the Doushantuo Formation are hollow is possibly due to the fact that they are mostly pyritized, i.e. most of the organic matter was decomposed. The small spheres were interpreted (Gan et al.,

2021) as possible spores, the larger ones were possibly symbiontic organisms living together with the fungi.

Myxomycetes (slime molds) are other possible eukaryots, which might have existed in the Proterozoic, although Stephenson et al. (2008) considered 50 My as the oldest fossil record. Their diverse morphology during the different stages of their life cycle including amoeboid forms leaves much room for speculation. Filamentous, mm-long sporocaps, such as shown in Fig. 3a in Rikkinen et al. (2019) are similar to what we see in Fig. 4b. The structured surfaces shown in Fig. 6 are somehow similar to what Dagamac et al. (2017) showed in their Figs. 7-9 from recent *Arcyria complex*, though on the µm-scale, whereas those from the Volyn biota are much larger. The image of multiple, conical filaments with claw-like ends, growing from a common center (Fig. 3j, k, l) is similar to *Copromyxa protea* shown by Schnittler et al. (2012) in their Fig. 4-2. Hollow objects (Fig. 7, i-k, m, n) resemble open sporocaps of liceaceae (Schnittler et al., 2012, in their Fig. 5-12). Finally, large objects such as the open, bowl-shaped one with bulbous outgrowths (Fig. 8) could be interpreted as plasmodium of a myxomycete with beginning development of fruiting bodies (e. g. Fig. 2, life cycle of myxomycetes, transition from stage H1 to A; Stephenson and Schnittler, 2016).

Other possible organisms described from the Precambrian are all very different from the Volyn biota and are excluded as possible analogues e.g. palynomorphs, which are among the earliest clear records of terrestrial life (Wellman and Strother, 2015); the 1.67 Ga eukaryotic Changcheng biota, (Miao et al., 2019), or vase-shaped metazoan microfossils, considered as the oldest evidence for heterotrophic protists, e.g. Urucum Formation, Brazil (Morais et al., 2017).

Most of the Precambrian biota listed in the literature are considered as photosynthetic organisms, probably not a likely analog for the Volyn biota. E. g. the 770 Ma (Cryogenian) Chichkan Fm. in Maly Karataou, Kazakhstan (Sergeev and Schopf, 2010) contains biota in fine-grained black chert, which were deposited in a mid-shelf and a near-shore environment with stromatolites. Most of the biota listed by Sergeev and Schopf (2010) are cyanobacteria, rather small mostly up to the 10 µm range and thus do not serve as analogues for the Volyn biota. They also list a number of larger protista (*incertae sedis*) in the 100 µm-range, however with little morphological similarity to the Volyn biota. No similarity was found to eukaryotes (acryitarchs) from 1.1 Ga old Taoudeni basin, Mauretania (Beghin et al., 2017). Red algae (rhodophytae) from the 1.05 Ga Hunting Fm, considered as among the oldest eukaryotes (Butterfield, 2000; Gibson et al., 2018) are photosynthetic organisms and can also be excluded.

**5.4 Model for a Precambrian deep biosphere ecosystem**

703 The Volyn occurrence is a well-preserved example of a fossil ecosystem of the deep continental
704 biosphere. We exclude an a-biotic origin as previously postulated (Ginzburg et al., 1987;
705 Lu'kyanova et al., 1992) because of the extremely low $\delta^{13}C$ values and the large variation in
706 morphology. A-biotic pseudofossils have been produced experimentally, e.g. by Nims et al.
707 (2021) and references therein, when sulfide is oxidized in the presence of organics. These
708 'organic biomorphs' show a large variety of morphologies, mostly filamentous, but also
709 globular. In a siliceous environment (for many cases chert) such organic biomorphs can be
710 replaced by silica, and their morphology can be well preserved. However, for the Volyn biota
711 such a sulfide rich environment did not exist. Additionally, we take the presence of chitosan as
712 another indication for a true fossil. McMahon (2019) provided another example of pseudo-
713 fossils, which is however restricted to an iron-rich environment; these pseudofossils consist of
714 hematite or Fe-oxides/hydroxides, conditions not realized in the highly differentiated
715 pegmatites, which are very poor in Fe. Rouillard et al. (2018) produced another type of
716 pseudofossils with an amazing large variety of morphologies, which might occur in
717 hydrothermal, silica-rich rocks, but requires a high activity of Ba, for which there is no
718 indication in the Volyn pegmatites.

719 In combination with textural arguments, the age determination of muscovite, formed in
720 pseudomorphs after beryl, points to a minimum age of 1.5 Ga (Franz et al., 2022b); the
721 maximum age is restricted by the intrusion of the igneous rocks at 1.760 Ga (Shumlyanksyy et
722 al., 2021).

723 The geological context argues for a continental, terrestrial environment, because the KPC
724 intruded into continental crust most likely in a within-plate tectonic setting (Shumlyanskyy et
725 al., 2012, 2017). After intrusion uplift to the erosion level occurred, documented by an
726 unconformity, and sedimentation started with sandstones and shales at approximately 1.4 Ga
727 (Zbranki Formation; Gorokov et al., 1981), later than or coeval with the pseudomorph
728 formation and the minimum age of the microfossils. The depth, where the organisms lived, is
729 an open question, but the occurrence in the underground mines indicate a depth of up to at least
730 150 m. The age of 1.5 Ga is much later than the Great Oxidation Event of the Earth's
731 atmosphere, allowing for the evolution of complex species and ecosystems on the land
732 (sub)surface. The supply of organic matter to the underground for the production of the high
733 amounts of kerite is speculative. In a geyser system, which we invoke for the whole geological
734 situation, intense growth of organisms at the surface is a common observation. In such systems
735 continuous exchange between surface and depth is evident. This also excludes very deep (more
736 than several hundreds of meters) biosphere. The biota was more likely located near to the

Gelöscht: ,

surface. Unfortunately, no information is available right now, which of the many pegmatites from the Volyn pegmatite field contains kerite and which – in what depth – are devoid of kerite. This remains to be investigated in the future.

Drake et al. (2017) reported partly mineralized fungi from the deep continental (granitic) biosphere (up to 740 m). The fossilization process also included maturation of the OM and final mineralization by clay minerals. The source of carbohydrates was living or dead bacterial biofilms, similar to what we speculate about the Volyn biota.

The large size of the filaments up to cm in length is a-typical for bacteria and archaea. Although Volland et al. (2022) described recent cm-long bacteria, these are still the exception, and it is more likely that some of the Volyn biota were multi-cellular eukaryotes. Their suggested age of 1.5 Ga is the age range given for the first appearance of eukaryotes (see review in Butterfield, 2015). Putative cm-sized Precambrian fossils (different from the Volyn biota) were reported from the 2.1 Ga old Francevillian biota (El Albani et al., 2014); however, they are completely pyritized and occur in diagenetically overprinted black shales, which makes the interpretation difficult.

The Volyn biota must have been highly radiation resistant, because a U-Th-K-rich granitic-pegmatitic system has a high radiation level. There are a number of different organisms, such as bacteria (e.g. *Deinococcus radiodurans*), archaea (*Thermococcus gammatolerans*) or microscopic fungi (e.g. *Cladosporium sphaerospermum*), which fulfill this requirement; see review in Matusiak (2019). During the mining operations in Soviet times, a high Rn content was measured inside cavities, when they were broken into. The general radiation levels, 3000 times higher than the allowed limit at that time, were even higher 1.5 billion years ago. Deeply black-colored quartz crystals in the pegmatites are of the 'morion' type and also indicate high radiation. Recent observations at the Tschernobyl power plant have led to the speculation about radiotrophic fungi (e.g. Matusiak, 2019; Prothmann and Zauner, 2014), which produce melanin as a protection against radiation and enhancement of fungal growth via capture of ionizing radiation for energy conversion (Dadachova et al., 2007; Tugay et al., 2017). Mycoremediation is at least a well-documented mechanism for a very effective method of radio nuclides pollutant removal considering the versatility of fungi in terms of their ecology, nutritional modes, adaptability, morphology, physiology, and metabolism (Shourie and Vijayalakshmi, 2022). Fungi are known as extremophylic organisms (e.g. Blachowicz et al., 2019) and we can expect that in the Proterozoic or possibly already earlier in Earth history similar organisms were active

and resistant to a high radiation level, in an epoch when the ozone layer was not yet fully developed.

## 6 Summary and conclusions

The exceptional 3D preservation of the 1.5 Ga Volyn biota is due to the fossilization conditions in open cavities, with $SiF_4$-rich fluids as the driving agent. There are a number of indications that fungi-like organisms were likely an important part of the microecosystem – hyphen with branching (though not anastomosing), growth in thinning-out ends, and also in bulbous extrusion, both at the end of filaments and along the filaments. Sheath-like structures are clearly visible, and there are good indications for a former biofilm and extracellular proteinic substance. The large size and internal structure of the organisms and the segmentation visible on thick filaments points to multicellular organisms, and the nano-sized inclusions of Bi(S,Te) crystals have an astonishingly good analog in recent fungi. Other organisms, which might have been present in this subsurface micro-ecosystem are myxomycetes or myxomycete-like. The stable N- and C-isotopic signature is in accordance with such an interpretation.

The fungi-like organisms possibly lived from lithotrophic methanogens; alternatively or additionally bacteria such as cyanobacteria were transported from the surface downwards into the cavities. The geyser system of the Korosten Pluton provided an ideal framework for growth of bacterial or algal organisms at the surface. In the deep biosphere, attached as well as free-living forms of organisms are observed.

The Volyn biota show that fungi-like organisms developed before 1 Ga (Loron et al.; 2019), and support the speculation that the fossils from the 2.4 Ga Ongeluk Formation were fungi-like organisms (Bengtson et al., 2017). Molecular clock data, especially the three-way split of the kingdoms animals-plants-fungi at 1.58±9 Ma (Wang et al., 1999) are still uncertain, but our data indicate that it must have occurred early in the Proterozoic.

The Volyn biota also prove that a deep continental biosphere was already present in the Early Mesoproterozoic/Late Paleoproterozoic. It is known that in the subseafloor environment microbial life existed in the Archean (Cavalazzi et al., 2021), as described from the 3.4 Ga old Onverwacht Group of the Barberton greenstone belt, but from the continental environment this has not yet been reported.

**Acknowledgements**

**Gelöscht:** benthic forms of the

**Gelöscht:** as well as organisms floating in water or growing in soft clay media, but not attached to the clay

**Formatiert:** Abstand Nach: 6 Pt.

**Gelöscht:** Furthermore, the Volyn biota must have been highly radiation resistant (e.g. the bacteria *Deinococcus radiodurans* or *Thermococcus gammatolerans*; see review in Matusiak, 2019), because a U-Th-K-rich granitic-pegmatitic system has a high radiation level. During the mining operations in Soviet times, a high Rn content was measured inside cavities, when they were broken into. The general radiation levels, 3000 times higher than the allowed limit at that time, were even higher 1.5 billion years ago. Deeply black-colored quartz crystals in the pegmatites are of the 'morion' type and also indicate high radiation. Recent observations at the Tschernobyl power plant have led to the speculation about radiotrophic fungi (e.g. Matusiak, 2019; Prothmann and Zauner, 2014), which produce melanin as a protection against radiation and enhancement of fungal growth via capture of ionizing radiation for energy conversion (Dadachova et al., 2007; Tugay et al., 2017). Mycoremediation is at least a well-documented mechanism for a very effective method of radio nuclides pollutant removal considering the versatility of fungi in terms of their ecology, nutritional modes, adaptability, morphology, physiology, and metabolism (Shourie and Vijayalakshmi, 2022). Fungi are known as extremophylic organisms (e.g. Blachowicz et al., 2019) and we can expect that in the Proterozoic or possibly already earlier in Earth history similar organisms were active and resistant to a high radiation level, in an epoch when the ozone layer was not yet fully developed. ¶

**Formatiert:** Großbuchstaben

We thank three anonymous reviewers for helpful and constructive suggestions, Tina Treude for editorial handling, Martin Schnittler for discussion and literature about myxomycetes, and Felix Haesler for discussion about fungi.

**Funding**

Alexander von Humboldt foundation provided support for VK during his stay in Berlin in 2022-2023.

**Author contribution**

Concept, writing, interpretation, EMPA and SEM data acquisition - GF; IR spectra, writing - VK; sampling and geological information - VC, PL; stable isotopes - US; SEM - UG; EMPA - JN.

**References**

Alleon, J., Bernard, S., Le Guillou, C., Beyssac, O., Sugitani, K., and Robert, F.; Chemical nature of the 3.4 Ga Strelley Pool microfossils, Geochem. Persp. Lett., 7, 37-42, 2018. doi 107185/geochemlet.1817.

Anwita, Gosh, S., Varma A. K., Das, S. K., Pal, D., and Solanki, G.: Metamorphic tranformations of nitrogen functionalities: Stabilization of organic nitrogen in anthracite and its effect on $\delta^{15}N$ parameter, Marine Petrol. Geol., 112, 2020. doi.org/10.1016/j.marpetgeo.2019.104090

Beghin, J., Storme, J.-Y., Blanpied, C., Gueneli, N., Brocks, J. J., Poulton, S. W., and Javaux, E. J.: Microfossils from the late Mesoproterozoic – early Neoproterozoic Atar/El Mreiti Group, Taudeni basin, Mauretania, northwestern Africa, Prec. Res. 291, 63-82, 2017.

Bengtson, S., Rasmussen, B., Ivarsson, M., Muhling, J., Broman, C., Marone, F., Stampanomi, M., and Bekker, A.: Fungus-like mycelial fossils in 2.4 billion-year-old vesicular basalt, Nature Ecol. Evol., 1(6), 1-6, 2017.

Berbee, M. L., Strullu-Derrien, C., Delaux, P.-M., Strother, P. K., Kenrick, P., Selosse, M.-A., and Taylor, J. W.: Genomic and fossil windows into the secret lives of the most ancient fungi, Nature Rev. Microbiol., 18, 717–730, 2020.

Blachowicz, A, Chiang, A. J., Elsaesser, A., Kalkum, M., Ehrenfreund, P., Totok, T., Wang, C. C. C., and Venkateswaran, K.: Protemoic and mteabolic characteristics of extremophilic fungi under simulated Mars conditions, Front. Microbiol. 10:1013, 2019, doi: 10.3389/fmicb.2019.01013

Budyak, A. E., and Brukhanova, N. N.: Selenium, bismuth, and mercury in black shale-hosted gold deposits of different genetic types, Geochem. Int., 50, 791-797, 2012.

Butterfield, N. J.: Bangiomorpha pubescens n. Gen., n. sp.: Implications for the evolution of sec, multicellularity, and the Mesoproterozoic/Neoproterozoic radiation of the eukaryotes, Paleobiol., 26, 386-404, 2000.

Butterfield, N. J.: Early evolution of the eukarya, Palaeontology, 58, 5-17, 2015. doi: 10.1111/pala.12139

Cavalazzi, B., Lemelle, L., Siminovici, A., Cady, S. L., Russell, M. J., Bailo, E., Canteri, R., Enrico, E., Manceau, A., Maris, A., Salomé, M., Thomassot, E., Bouden, N., Tucoulou, R., and Hofman, A.: Cellular remains in a ~3.42-billion-year-old subseafloor hydrothermal

environment, Sci. Adv., 7, eabf3963, 2021.
Coates J.: Interpretation of infrared spectra, a practical approach, Encyclopedia of Analytical Chemistry R.A. Meyers (Ed.), copyright John Wiley & Sons Ltd., 2011.
Dadachova, E., Bryan, R. A., Huang, X., Moadel, T., Schweitzer, A. D., Aisen, P., Nosanchuck, J. D., and Casedevall, A.: Ionization radiation changes the electronic properties of melanin and enhances the growth of melanized fungi, PLoS ONE, 5, 1-13, 2007.
Dagamac, N. H., Dela Cruz, T. E., Rea-Maninta, M. A. D., Aril-Dela Cruz, J. V., and Schnittler, M.: Rapid assessment of myxomycete diversity in the Bicol Peninsula, Phillipines, Nova Hedwigia, 104. 1-3, 31-46, 2017.
El Albani, A., Bengtson, S., Canfield, D. E., Riboulleau, Bard, C. R., et al.: The 2.1 Ga old Francevillian biota: Biogenecity, taphonomy and biodiversity, PLoS ONE 9(6): e99438, 2014. doi: 10.1371/journal.pone.0099438.
Finkelman, R. B., Dai, S., and French, D.: The importance of minerals in coal as the hosts of chemical elements: A review, Int. J. Coal Geology, 212, 103251, 2019.
Fischer, R., Zekert, N., and Takeshita, N.: Polarized growth in fungi – interplay between the cycloskeleton, positional markers and membrane domains, Molec. Microbiol., 68, 813-826, 2008.
Franz, G. Khomenko, V. Vishnyevskyy, A. Wirth, R. Nissen, J. Rocholl A.: Biologically mediated crystallization of buddingtonite in the Paleoproterozoic: Organic-igneous interactions from the Volyn pegmatite, Ukraine, Amer. Mineral. 102, 2119-2135, 2017.
Franz, G., Lyckberg, P., Khomenko, V., Chournousenko, V., Schulz, H.-M., Mahlstedt, N., Wirth, R., Glodny, J., Gernert, U., and Nissen, N.: Fossilization of Precambrian organic matter (kerite) from the Volyn pegmatite, Ukraine, BioGeosci., 19, 1795-1811, 2022a.
Franz, G., Sudo, M., Khomenko, V.: $^{40}Ar/^{39}Ar$ dating of a hydrothermal pegmatitic buddingtonite-muscovite assemblage from Volyn, Ukraine, Eur. J. Mineral., 34, 7-18, 2022b. doi.org/10.5194/ejm-34-7-2022.
Gan, T., Luo, T., Pang, K., Zhou, Ch., Zhou, G., Wan, B., Li, G., Yi, Q., Czaja, A. D. and Xiao, S.:Cryptic terrestrial fungus-like fossils of the early Ediacaran Period, Nature Comm., doi.org/10.1038/s41467-021-20975-1, 2021.
Gibson, T. M., Shih, P. M., Cumming, V. M., Fischer, W. W., Crockford, P. W., Hdgekiss, M. S. W., Wörndle, S., Creaser, R. A., Rainbird, R. H., Skulski, T. M., and Halverson, G. P.: Precise age of Bangiomorpha pubescens dates the origin of eurkaryotic photosynthesis, Geology, 46, 135-138, 2018.
Ginzburg, A. I., Bulgakov, V. S., Vasilishin, I. S., Luk'yanova, V. T., Solntseva, L. S., Urmenova, A. M., and Uspenskaya, V. A.: Kerite from pegmatites of Volyn, Dokl. Akad. Nauk SSSR, 292, 188–191, 1987, (in Russian).
Gorlenko, V.M., Zhmur, S.I., Duda, V.I., Osipov, G.A., Suzina, N.E., and Dmitriev, V. V.: Fine structure of fossilized bacteria in Volyn kerite, Orig. Life Evol. Biosph., 30, 567–577, 2000.
Gorokov, I. M., Clauer, N., Varshavskaya, E. S., Kutyavin, E. P., and Drannik, A. S.: Rb-Sr ages of Precambrian sediments from the Ovruch Mountain range, Northwestern Ukraine (U.S.S.R.), Precam. Res., 6, 55-65, 1981.
Hall-Stoodley, L., Costerton, J. W., and Stoodley, P.: Bacterial biofilms: From the natural environment to infectious diseases, Nature Rev. Microbiol., 2, 95-108, 2004.
Högberg, P., Plamboeck, A. H., Taylor, A. F. S., and Fransson, P. M. A.: Natural $^{13}C$ abundance reveals trophic status of fungi and host-origin of carbon in mycorrhizal fungi in mixed forests, Proc. Natl. Acad. Sci. USA, 96, 8534-8539, 1999.
Ivanovich, P. V., and Alekseevich, D. S.: Mineralogy of the Volynian chamber pegmatites, EKOST Association, Mineral. Almanac, 12, 128 p, Moscow, 2007.
Krings, M., Taylor, T. N., and Dotzler, N.: Fossil evidence of the zygomycetous fungi, Persoonia, 30, 1-10, 2013.

927 Lepot, K., Williford, K. H., Ushikubo, T., Sugitani, K., Mimura, K., Spicuzza, M. J., and
928 Valley, J. W.:Texture-specific isotopic compositions in 3.4 Gyr old organic matter support
929 selective preservation in cell-like structures, Geochim. Cosmochim. Acta, 112, 66-86, 2013.
930 Li J., Zhang L.-P., Peng F., Bian J., Yuan T.-Q., Xu F., Sun R.-C.: Microwave-assisted solvent-
931 free acetylation of cellulose with acetic anhydride in the presence of iodine as a catalyst,
932 Molecules, 14, 3551-3566, 2009. doi:10.3390/molecules14093551.
933 Liang, X., Perez, M. A. M.-J., Nwoko, K. C., Egbers, P., Feldmann, J., Csentenyi, L., and Gadd,
934 G. M.: Fungal formation of selenium and tellurium nanopartikels, Appl. Microbiol. Biotechn.,
935 103, 7241-7259, 2019.
936 Liang, X., Perez, M. A. M.-J., Zhang, S., Song, W., Armstrong, J. G., Bullock, L. A., Feldmann,
937 J., Parnell, J., Csentyi, L., and Gadd, G. M.: Fungal transformation of selenium and tellurium
938 located in a volcanogenic sulfide deposit, Environ. Microbiol., 22, 2346-2364, 2020.
939 Loron, C. C., François, C., Rainbird, R. H., Turner, E. C., Borensztajn, S., and Javaux, E. J.:
940 Early fungi from the Proterozoic era in Arctic Canada, Nature, 570.7760: 232-235, 1992.
941 Lu'kyanova, V. T., Lobzova, R. V., and Popov, V. T.: Filaceous kerite in pegmatites of Volyn,
942 Izvestiya Ross. Akad. Nauk Ser. Geologicheskaya, 5, 102-118 (in Russian), 1002.
943 Lutzoni, François, Michael D. Nowak, Michael E. Alfaro, Valérie Reeb, Jolanta
944 Miadlikowska, Michael Krug, A. Elizabeth Arnold et al.: Contemporaneous radiations of
945 fungi and plants linked to symbiosis, Nature Comm. 9, no. 1, 1-11, 2018.
946 Lyckberg, P., Chornousenko, V., and Wilson, W. E.: Famous mineral localities: Volodarsk-
947 Volynski, Zhitomir Oblast, Ukraine, The Mineral. Record, 40, 473-506, 2009.
948 Lyckberg, P., Chournousenko, V., and Chournousenko, O.: Giant heliodor and topaz pockets
949 of the Volodarsk chamber pegmatites, Korosten pluton, Ukraine, 36th Intern. Gemm. Conf.,
950 Nantes, France, Abstr. vol., 78-83, 2019.
951 McMahon, S.:Earth's earliest and deepest purported fossils may be iron-mineralized chemical
952 gardens, Porceedings of the Royal Society, B 286, 2018.
953 http://dx.doi.org/10.1098/rspb.2019.2410.
954 Mariotti, A.: Atmospheric nitrogen is a reliable standard for natural $^{15}N$ abundance
955 measurements, Nature, 303(5919), 685-687, 1983.
956 Mayor, J. R., Schuur, E. A. G., and Henkel, T. W.: Elucidating the nutritional dynamics of fungi
957 using stable isotopes, Ecology Lett., 12, 171-183, 2009.
958 Matusyak, D. M.: Radiotolerant microorganisms – characterization of selected species and their
959 potential usage, Adv. Microbiol., 55, 182-194, 2016.
960 Miao, L. Y., Moczydłowska, M., Zhu, S. X. and Zhu, M. Y.: New record of organic- walled,
961 morphologically distinct microfossils from the late Paleoproterozoic Changcheng Group in
962 the Yanshan Range, North China, Precam. Res., 321, 172–198, 2019.
963 Missen, O. P., Ram, R., Mills, S. J., Etschmann, B., Reith, F., Shuster, J., Smith, D., J., and
964 Brugger, J.: Love is in the Earth: A review of tellurium (bio)geochemistry in surface
965 environments, Earth Sci. Rev., 2020, doi.org/10.1016/j.earthscirev.2020.103150.
966 Morais, L., Fairchild, T. R., Lahr, D. J. G., Rudnitzki, I. D., Schopf, J. W., Garcia, A. K.,
967 Kudryavtsev, A. B., and Romero, G. R.: Carbonaceous and siliceous Neoproterozoic vase-
968 shaped microfossils (Urucum Formation, Brazil) and the question of early protistan
969 biomineralization, J. Paleontol., 91(3), 393-406, 2017. doi: 10.1017/jpa.2017.16.
970 Nakamoto K.: Infrared spectra of inorganic and coordination compounds, Parts A and B. New
971 York: Wiley, p. 328., John Wiley & Sons, New York, 1997.
972 Nims, C., Lafond, J., Alleon, J., Templeton, A. S., and Cosmidis, J.: Organic biomorphs may
973 be better preserved than mircoorganisms in the early Earth sediments, Geology, 49, 629-634,
974 2021. https://doi.org/10.1130/G48152.1.
975 Petersen, B. M., and Fry, B.: Stable isotopes in ecosystem studies, Ann. Rev. Ecology System.,
976 18, 293-320, 1987.

977 Prothman, C., and Zauner, K.-P. Semibiotic Persistence, J. Brit. Interplanet. Soc. (JBIS), 67(7-
978 9), 314-321, 2014 doi://www.jbis.org.uk/paper.php?p=2014.67.314.
979 Rasmussen, B., Blake, T. S., Fletcher, I. R., and Kilbum, M. R.: Evidence for microbial life in
980 synsedimentary cavities from 2.75 Ga terrestrial environments, Geology, 37, 423-426, 2009.
981 Rikkinen, J., Grimaldi, D. A., and Schmidt, A.; Morphological stasis in the first myxomycete
982 from the Mesozoic, and the likely role of cryptobiosis, Scientific Reports 9.1, 19730, 2019.
983 Roulliard, J., García-Ruiz, J.-M., Gong, J., and van Zuilen, M. A.: A morphogram for silia-
984 witherite biomorphs and its application to microfossil identification in the early earth rock
985 record, Geobiology, 16, 279-296. 2018. doi.org/10.1111/gbi.12278.
986 Schnittler, M. Novozhilov, Y. K., Romeralo, M., Brown, M., and Spiegel, F. W.: Fruit body-
987 forming protists: Myxomycetes and Myxomycete-like organisms, chapter 4, 40-88, in: Engler,
988 A., and Frey, W., Syllabus of Plant Families-A. Engler's Syllabus der Pflanzenfamilien Part
989 1/1, Stuttgart: Bornträger, 2012.
990 Sergeev, V. N., and Schopf, J. W.: Taxonomy, paleoecology and biostratigraphy of the Late
991 Neoproterozoic Chichkan microbiota of South Kazakhstan: The marine biosphere on the eve of
992 metazoan radiation, J Paleont., 84, 363-401, 2010
993 Shourie, A., and Vijayalakshmi U.: Fungal diversity and its role in mycoremediation,
994 Geomicrobiol. J., 39, 3-5, 426-444, 2022, doi.org/10.1080/01490451.2022.2032883.
995 Shumlyanskyy, L., Billström, K., Hawkesworth, C., and Elming, S.-Å.: U-Pb age and Hf
996 isotope compositions of zircons from the north-western region of the Ukranian shield: mantle
997 melting in response to post-collision extension. Terra Nova 24, 373-379, 2012.
998 Shumlyanskyy L., Hawkesworth C., Billström K., Bogdanova S., Mytrokhyn O., Romer R.,
999 Dhuime B., Claesson S., Ernst R., Whitehouse M., Bilan O.: The origin of the Palaeoproterozoic
1000 AMCG complexes in the Ukrainian Shield: new U-Pb ages and Hf isotopes in zircon, Precam.
1001 Res., 292, 216-239, 2017.
1002 Shumlyanskyy, L., Franz, G., Glynn, S., Mytrokhyn, O., Voznyak, D., and Bilan O.:
1003 Geochronology of granites of the western part of the Korosten AMCG complex (Ukrainian
1004 Shield): implications for the emplacement history and origin of miarolitic pegmatites, Eur. J.
1005 Min., 33, 703-716, 2021.
1006 Stephenson, S. L., Schnittler, M., and Nvozhilov, Y. K.: Myxomycete diversity and distribution
1007 from the fossil record to the present, Biodivers. Conserv, 17, 285-301, 2008. Doi.org
1008 10.1007/s10531-007-9252-9.
1009 Stephenson, S. L., and Schnittler, M., Myxomycetes, in:Archibald et al. (eds.) Handbook of the
1010 protists, 1-26, Springer International Publishing AG 2016. doi.org 10.1007/978-3-319-32660-
1011 6_44-1.
1012 Struck, U.: On the use of stable nitrogen isotopes in present and past anoxic environments. In:
1013 Altenbach, A. V., Bernard, J. M. and Seckbach, J. (eds.) Anoxia, evidence for eukaryote
1014 survival and paleontological strategies. Book series: Cellular origin, life in extreme habitats and
1015 astrobiology, 21, 497-513, Springer, Berlin, 2012.
1016 Tugay, T., Zhdanova, N.N., Zheltonozhsky, V., Sadovnikov, L., and Dighton, J.: The influence
1017 of ionizing radiation on spore germination and emergent hyphal growth response reactions of
1018 microfungi, Mycologia, 98, 4, 521-527, 2006/2017.
1019 doi.org/10.1080/15572536.2006.11832654.
1020 Vasilev, A., Efimov, M., Bondarenko, G., Kozlov, V., Dzidziguri, E., and Karpacheva, G.:
1021 Thermal behavior of chitosan as a carbon material precursor under IR radiation, IOP Conf. Ser.:
1022 Mater. Sci. Eng. 693, 2019. doi.org/10.1088/1757-899X/693/1/012002.
1023 Volland, J.-M., Gonzalez-Rizzo, S., Gros, O., Tyml, T., Ivanova, N., Schulz, F., Goudeau, D.
1024 et al.: A centimeter-long bacterium with DNA contained in metabolically active, membrane-
1025 bound organelles. Science, 376.6600, 1453-1458, 2022. doi.org/10.1126/science.abb3634.
1026 Wanjun T., Cunxin W., Donghua, C.: Kinetic studies on the pyrolysis of chitin and chitosan,
1027 Polym. Degrad. Stabil. 87, 389–394, 2005.

1028 Wang, D. Y.-C., Kumar, S., and Hedges, S. B.: Divergence time estimates for the early history
1029 of animal phyla and the origin of plants, animals and fungi, Proc. R. Soc. Lond., 266, 163-171,
1030 1999.
1031 Wellman, C. H., and Strother, P. K.: The terrestrial biota prior to the origin of land plants
1032 (embryophytes): A review of the evidence, Paleontol., 58, 601-627, 2015.
1033 Westall, F., de Witt, M. J., Dann, J., van der Gaast, S. de Ronde, C. E.J., and Gerneke, D.: Early
1034 Archean fossil bacteria and biofilms in hydrothermally-influenced sediments from the
1035 Barberton greenstone belt, South Africa. Prec. Res., 106, 93-116, 2001.
1036 Zawadzki, J., and Kaczmarek, H.: Thermal treatment of chitosan in various conditions,
1037 Carbohydr. Polym., 80, 394-400, 2010.
1038 Zhmur, S. I.: Origin of Cambrian fibrous kerites of the Volyn region, Lithol. Mineral Resour.,
1039 38, 55-73, 2003.